

# Exact Solutions for a GBM-type Stochastic Volatility Model having a Stationary Distribution

Alan L. Lewis\*

May 28, 2019

## Abstract

We find various exact solutions for a new stochastic volatility (SV) model: the transition probability density, European-style option values, and (when it exists) the martingale defect. This may represent the first example of an SV model combining exact solutions, GBM-type volatility noise, and a stationary volatility density.

## 1 Introduction

We develop the following stochastic volatility (SV) model for the real-world (P-measure) evolution of a financial asset  $S_t$ , such as a broad-based stock index:

$$\text{Under P : } \begin{cases} dS_t = (\alpha + \beta \sigma_t^2) S_t dt + \sigma_t S_t dB_t, & S_t \in \mathbb{R}_+, \\ d\sigma_t = \sigma_t(\omega - \theta \sigma_t) dt + \xi \sigma_t dW_t, & \sigma_t \in \mathbb{R}_+, \\ dB_t dW_t = \rho dt. \end{cases} \quad (1)$$

Here  $(B_t, W_t)$  are correlated Brownian motions with correlation  $\rho$ . Also  $(\alpha, \beta, \omega, \theta, \xi, \rho)$  are constant parameters of the model, meant to be estimated from financial time series. We generally assume throughout that  $(\omega, \theta, \xi^2) > 0$ , although we sometimes admit  $\omega = \theta = 0$  or even  $\theta < 0$ .

We also develop a risk-neutral (Q-measure) version of the model, which is used for option valuation. In that one,  $\alpha$  becomes a cost-of-carry:  $\alpha \rightarrow (r - q)$ , where  $r$  is an interest rate and  $q$  is a dividend yield. In addition,  $\beta \rightarrow 0$ , and  $\omega \rightarrow \omega_Q$ , (a possibly different parameter) while the other parameters  $(\theta, \xi, \rho)$  remain identical to their P-measure values.

An attractive feature of the model is that the stochastic volatility  $\sigma_t$  is driven by a geometric Brownian motion (GBM)-type noise. GBM volatility seems to be favored by time series analysis over the “square-root” variance noise of popular affine-type diffusion models, such as the Heston '93 model.<sup>1</sup> Extended with the drifts shown, I call it the ‘Extended GBM’ model, or XGBM for short.

\*Newport Beach, California, USA; email: alewis@financepress.com

<sup>1</sup>See, for example [2] and [10].

As we show, the model admits an exact solution for the transition density, vanilla option values, and some other quantities of interest. In these solutions, we find two qualitatively different regimes:

- Case 1:  $\frac{1}{2}\xi^2 \leq \omega < \infty$ ,
- Case 2:  $0 \leq \omega < \frac{1}{2}\xi^2$ .

In Case 1, the driving volatility process is mean-reverting and has a stationary density. In Case 2, with probability 1, as  $t$  grows large  $\sigma_t \rightarrow 0$ , similar to the SABR model. Indeed, the lognormal SABR model is a special case of (1) when the drifts are absent.

However, a weakness of the SABR model is its lack of a stationary density for the volatility. Thus (under Case 1), we have here what may represent the first example of an SV model combining: GBM-type volatility noise, a stationary volatility density, and exact solutions.

Numerically, we find option values (and thus implied volatilities) continuous vs.  $\omega$ , including at the borderlines case:  $\omega = \frac{1}{2}\xi^2$ .

In brief, the problem is solvable because it is reducible to the evolution problem for a 1D diffusion operator admitting a spectral expansions in terms of confluent hypergeometric functions  $M(a, b, x)$  and  $U(a, b, x)$ . The other special function that will appear frequently is

$$F(a, b, c; z) = \sum_{n=0}^{\infty} \frac{(a)_n (b)_n}{(c)_n} \frac{z^n}{n!},$$

the Gauss hypergeometric function. The  $(a)_n$  etc are Pochhammer symbols. All these functions are built-in in Mathematica, where everything is implemented.

Structurally, the model is similar to the one-factor short-term interest rate model,  $dr_t = r_t(\omega - \theta r_t) dt + \xi r_t dW_t$ , originally due to Merton and which I fully solved in [4] (reprinted in [6]). The solvability of Merton's model suggests, but does not prove, that associated 2D SV models such as (1) are also solvable. Another suggestion that my XGBM SV model might be solvable is the discussion found in [3] (Sec. 9.5).

As it turns out, moving from the interest rate model to the associated stochastic volatility model is tricky. One reason is the “reduced” PDE coefficients become complex-valued, which complicates the associated spectral expansion. Another reason is that the “fundamental transform” needed for option valuation (using the language of [5]) requires a regularization for Case 2. All that is explained below; key formulas are boxed.

## 2 The Joint Transition Probability Density

With  $(X_t, Y_t) := (\log S_t, \sigma_t)$  the system (1) reads:

$$\begin{cases} dX_t = [\alpha + (\beta - \frac{1}{2}) Y_t^2] dt + Y_t dB_t, & X_t \in \mathbb{R}, \\ dY_t = (\omega Y_t - \theta Y_t^2) dt + \xi Y_t dW_t, & Y_t \in \mathbb{R}_+, \\ dB_t dW_t = \rho dt. \end{cases} \quad (2)$$

We seek the bivariate transition probability density  $p(t, x', y'|x, y)$  defined by  $p(t, x', y'|x, y) dx' dy' = \mathbb{P}(X_t \in dx', Y_t \in dy' | X_0 = x, Y_0 = y)$ . The initial condition is  $p(0, x', y'|x, y) = \delta(x' - x) \delta(y' - y)$ , using the Dirac delta. All parameters are real; assume  $(\omega, \theta) \geq 0$ . Using subscripts for derivatives, the corresponding Kolmogorov backward PDE problem is

$$\begin{cases} p_t = \frac{1}{2} y^2 (p_{xx} + 2\rho\xi p_{xy} + \xi^2 p_{yy}) + [\alpha + (\beta - \frac{1}{2}) y^2] p_x + (\omega y - \theta y^2) p_y, \\ p(0, x', y'|x, y) = \delta(x - x') \delta(y - y'). \end{cases} \quad (3)$$

The system (2) is a MAP (Markov Additive Process), where  $X_t$  is the additive component and  $Y_t$  is the Markov component. This is also seen in the  $x$ -independence in the coefficients of (3). The MAP property implies  $p(t, x', y'|x, y) = p(t, x' - x, y'|0, y)$  which in turn implies the existence of a Fourier representation:

$$p(t, x', y'|x, y) = \int_{-\infty}^{\infty} e^{-iz(x' - x)} \Phi(t, z, y, y') \frac{dz}{2\pi}, \quad (4)$$

for a characteristic function  $\Phi$  to be determined below.

In the Heston '93 model (also a MAP),  $\Phi$  is found in terms of Bessel functions. Here the situation is not quite so simple: we'll find that  $\Phi$  itself requires an integration using confluent hypergeometric functions  $M(a, b, x)$  and  $U(a, b, x)$ . The additional integration means that numerical evaluations of the exact formulas will take an order of magnitude more computer time than Heston. Pure numerics, such as a PDE approach, will be similar in the two models.

## 2.1 Reduction to an auxiliary problem for $G(\tau, y, y')$

Because of the MAP property it suffices to solve (3) with  $x' = 0$ . Let  $\Phi(t, y, y') = \int e^{-1zx} p(t, 0, y'|x, y) dx$ , suppressing the display of the  $z$  dependence. Applying  $\int e^{-1zx}(\dots) dx$  to both sides of (3) and using parts integrations (the boundary terms vanish) yields:

$$\begin{cases} \Phi_t = \frac{1}{2}\xi^2 y^2 \Phi_{yy} + b(y; z)\Phi_y - c(y; z)\Phi, \\ \Phi(0, y, y') = \delta(y - y'), \end{cases} \quad (5)$$

where  $b(y; z) = \omega y - (\theta - 1z\rho\xi)y^2$  and  $c(y; z) = -1z\alpha + [\frac{1}{2}z^2 - 1z(\beta - \frac{1}{2})]y^2$ .

Letting  $\Phi(t, y, y') = e^{1z\alpha t} G(\tau, y, y'; z)$ , where  $\tau = \frac{1}{2}\xi^2 t$  yields

$$\begin{cases} G_\tau = y^2 G_{yy} + (\tilde{\omega}y - \theta_z^- y^2)G_y - c_z^+(\beta)y^2 G, \\ G(0, y, y') = \delta(y - y'), \end{cases} \quad (6)$$

introducing  $\tilde{\omega} = \frac{2\omega}{\xi^2}$ ,  $\theta_z^- = \frac{2}{\xi^2}(\theta - 1z\rho\xi)$ , and  $c_z^+(\beta) = \frac{2}{\xi^2}[\frac{1}{2}z^2 - 1z(\beta - \frac{1}{2})]$ .

The  $\pm$  superscripts on  $\theta_z$  and  $c_z$  distinguish them from similar expressions introduced later where the sign of  $z$  is flipped from the convention here. The mnemonic is that  $\theta_z^-$  indicates that  $z$  occurs as  $-1z$ , so the sign is *minus*. That is,  $\theta_z^\pm := \frac{2}{\xi^2}(\theta \pm 1z\rho\xi)$ . The sign on  $c_z^+(\beta)$  refers to the risk-neutral case where  $\beta = 0$ ; i.e.,  $c_z^\pm(0) = (z^2 \pm 1z)/\xi^2$ .

As we see, starting from real  $(\omega, \theta) \geq 0$ , and regardless of the  $\pm$  superscripts, the reduced problems have real  $\tilde{\omega} \geq 0$ , while  $(\theta_z, c_z) \in \mathbb{C}$ . If the Fourier inversion is performed along the real  $z$ -axis, and of course  $\beta$  is real, we also have  $\Re \theta_z \geq 0$  and  $\Re c_z \geq 0$ . In terms of  $G$ , (4) reads:

$$p(t, x', y'|x, y) = \int_{-\infty}^{\infty} e^{-1z(x' - x - \alpha t)} G(\frac{1}{2}\xi^2 t, y, y'; z) \frac{dz}{2\pi}, \quad (7)$$

We call  $G$  the (auxiliary model) Green function, although we may also refer to its Laplace transform as a Green function.

## 2.2 Spectral expansion for $G$ (overview)

Suppressing the  $z$ -dependence,  $G(\tau, y, y')$  has a Laplace transform with respect to  $\tau$ , call it  $\hat{G}(s, y, y')$ , where  $s$  is the transform variable. When we invert the transform via a Bromwich contour in the complex  $s$ -plane, we'll discover various singularities which are associated to the spectrum. See Fig. 1 for a typical case.

The simplest situation has real parameters,  $(\omega, \theta, c) \geq 0$ . Then, we'll find that  $\hat{G}(s, y, y')$  has

1. A branch cut singularity at  $s = s_c := -\frac{1}{4}(\omega - 1)^2$ .
2. A set of poles (or sometimes an empty set) at  $s_n, (n = 0, 1, \dots, n_{max})$ . These poles are a finite set of non-positive reals, lying in  $s \in (s_c, 0)$ .

The net result of the Laplace inversion is a spectral expansion of the form:

$$G(\tau, y, y') = 1_{pc} \sum_{n=0}^{n_{max}} \phi_n(y, y') e^{s_n \tau} + e^{s_c \tau} \int_0^\infty \phi_\nu(y, y') e^{-\nu^2 \tau} d\nu, \quad (8)$$

The specifics are given in Sec. 2.3 and developed in detail in Appendix A..

The poles generate the discrete spectrum and the discrete sum term in (8). Here  $1_{pc}$  denotes a ‘‘pole condition’’, which is a criterion on the parameters for the discrete contribution to appear at all. This term may be absent.

The branch cut singularity marks the right edge of the  $s$ -plane interval  $(-\infty, s_c)$ , which is the continuous spectrum, leading to the integral term in (8). This term is always present.

As we saw in Sec. 2.1, for XGBM we need  $\omega \geq 0$ , but  $(\theta, c) \rightarrow (\theta_z, c_z)$ , complex functions of the Fourier parameter  $z$ . In that case, the general form (8) still holds, but the structure of the spectrum is altered. A continuous spectrum remains along  $(-\infty, s_c)$ . However, the poles generally leave the real  $s$ -axis, as illustrated in Fig. 1. The figure illustrates two poles, shown as the ‘crossed-circles’.

Indeed, since (complex)  $z$  varies continuously under a Fourier inversion, we have *pole trajectories*  $s_n(z)$ . Examples are shown in Fig. 2 for a case with (initially) three poles. The illustrated trajectories start in the real interval  $(s_c, 0)$  as in the real parameter case, then leave the real  $s$ -axis, and finally return to touch the branch cut – at which point they leave the discrete spectrum. In turn, this leads to other complications which are seen in Fig. 3 and discussed later. Overall, the complex parameter case is, well, complex!

### 2.3 Spectral expansion for $G$ (result)

As shown, the transition density we seek is found in terms of a Green function for an auxiliary 1D PDE with (two) complex coefficients. Simplifying the notation, the reduced problem (6) reads:

$$\begin{cases} G_\tau = y^2 G_{yy} + (\omega y - \theta y^2) G_y - cy^2 G, \\ G(0, y, y') = \delta(y - y'). \end{cases} \quad (9)$$

As before, real  $\omega \geq 0$ , while  $(\theta, c) \in \mathbb{C}$  with  $\Re c \geq 0$ . Solving (9) is the key to the XGBM model. From that solution, all the other results in this article follow. I find:

**Theorem 1** (auxiliary Green function). *Let  $[x]$  denote the greatest integer in  $x$ ,  $(a)_n = a(a+1)\cdots(a+n-1)$  is the Pochhammer symbol, and the further notations*

$$\gamma = -\frac{1}{2}(\theta - \sqrt{\theta^2 + 4c}), \quad R = \theta + 2\gamma, \quad \psi = \frac{\omega\gamma}{R}, \quad r_n = -(n + \psi),$$

$$s_n = (n + \psi)^2 + (1 - \omega)(n + \psi), \quad b_n = \omega + 2r_n, \quad a_\nu = \frac{1}{2}(1 - \omega) + \psi + i\nu, \quad b_\nu = 1 + 2i\nu.$$

Assume real  $\omega \geq 0$ , while  $(\theta, c) \in \mathbb{C}$  with  $\Re c \geq 0$ . Then, the spectral representation solution to PDE problem (9) is given by

$$\boxed{G(\tau, y, y'; \omega, \theta, c) = R(Ry')^{\omega-2} e^{-\gamma y} e^{-(\theta+\gamma)y'} \times \mathbf{1}_{\{\frac{\omega-1}{2} > \Re\psi\}} \sum_{n=0}^{[(\omega-1)/2 - \Re\psi]} \phi_n(y, y') e^{s_n \tau} + (y')^{\omega-2} (yy')^{(1-\omega)/2} e^{-\gamma y} e^{-(\theta+\gamma)y'} e^{-(1-\omega)^2 \tau/4} \int_0^\infty \phi_\nu(y, y') e^{-\nu^2 \tau} d\nu,} \quad (10)$$

where

$$\phi_n(y, y') = \frac{(\omega - 1 - 2n - 2\psi)(b_n)_n}{n! \Gamma(b_n)} (R^2 yy')^{r_n} M(-n, b_n, Ry) M(-n, b_n, Ry')$$

and

$$\phi_\nu(y, y') = \frac{1}{2\pi} \frac{\Gamma(a_\nu) \Gamma(a_{-\nu})}{|\Gamma(2i\nu)|^2} (R^2 yy')^{i\nu} U(a_\nu, b_\nu, Ry) U(a_\nu, b_\nu, Ry').$$

Proof: In outline, we construct the solution by Laplace transform of (9) with respect to  $\tau$ . This leads to an ODE reducible to Kummer's differential equation, with Laplace transform parameter  $s$ . The ODE solution  $\hat{G}(s, y, y')$  is constructed; we perform the Laplace inversion by a Bromwich contour, which yields a first solution for  $G$ . Finally the spectral representation (10), which is a second solution for  $G$ , is found by applying the Residue Theorem to the Bromwich inversion. Details are found in Appendix A.

## 2.4 Summary for the transition density

To summarize at this point, the transition density for the P-model XGBM system (2) is given by

$$\begin{aligned}
 p_{XGBM}(t, x', y' | x, y) &= \int_{-\infty}^{\infty} e^{-1z(x'-x-\alpha t)} G\left(\frac{1}{2}\xi^2 t, y, y'; \tilde{\omega}, \theta_z^-, c_z^+\right) \frac{dz}{2\pi}, \\
 \text{where } \tilde{\omega} &= \frac{2\omega}{\xi^2}, \quad \theta_z^- = \frac{2}{\xi^2}(\theta - 1z\rho\xi), \quad c_z^+ = \frac{2}{\xi^2}\left(\frac{1}{2}z^2 - 1z(\beta - \frac{1}{2})\right), \\
 \text{and } G(t, y, y'; \omega, \theta, c) &\text{ is given at (10).}
 \end{aligned}
 \tag{11}$$

For numerics, it is more efficient to use

$$p_{XGBM}(t, x', y' | x, y) = \int_0^{\infty} \Re \left\{ e^{-1z(x'-x-\alpha t)} G\left(\frac{1}{2}\xi^2 t, y, y'; \tilde{\omega}, \theta_z^-, c_z^+\right) \right\} \frac{dz}{\pi}.$$

## 2.5 Spectral expansion for $G$ (special cases)

### 2.5.1 The stationary limit.

Suppose  $\omega > 1$ ,  $\theta > 0$ , and  $c = 0 \Rightarrow \gamma = \psi = 0$ . In the large  $\tau$  limit, (10) yields

$$\Psi(y') := \lim_{\tau \rightarrow \infty} G(\tau, y, y') = \frac{\theta (\theta y')^{\omega-2}}{\Gamma(\omega-1)} e^{-\theta y'}, \quad (\omega > 1). \tag{12}$$

This is the stationary density for the (standardized) stand-alone volatility process; i.e., when  $\xi^2 = 2$ . When  $0 \leq \omega \leq 1$ , then (10) still holds without a stationary limit. In that case, the  $Y_t$  particle mass eventually accumulates arbitrarily close to  $Y = 0$ . For general  $\xi^2$ , (12) holds with

$$(\omega, \theta) \rightarrow (\tilde{\omega}, \tilde{\theta}) := \frac{2}{\xi^2}(\omega, \theta) \text{ and } \mathbb{E}[\sigma_{\infty}] = \int y \Psi(y) dy = \frac{\tilde{\omega}-1}{\tilde{\theta}}, \quad (\tilde{\omega} > 1). \tag{13}$$

### 2.5.2 The norm-preserving case: $c = 0$ .

Suppose  $(\omega, \theta) > 0$  in (9) are real and  $c = 0$ . With no killing, the Green function should be norm-preserving on  $\mathbb{R}_+$ :  $\int_0^{\infty} G(t, y, y') dy' = 1$ . Let's check that for the sub-case  $\omega > 1$ .

With  $c = 0$  and  $\theta > 0$ , then  $\gamma = \psi = 0$ . Then, using the stationary density from (12), Theorem 1 reads:

$$\begin{aligned}
 G(\tau, y, y') &= 1_{\{\omega > 1\}} \left[ \Psi(y') + \theta (\theta y')^{\omega-2} e^{-\theta y'} \sum_{n=1}^{[(\omega-1)/2]} \phi_n(y, y') e^{s_n \tau} \right] \\
 &+ (y)^{(1-\omega)/2} (y')^{-3/2+\omega/2} e^{-\theta y'} e^{-(1-\omega)^2 \tau/4} \int_0^{\infty} \phi_{\nu}(y, y') e^{-\nu^2 \tau} d\nu, \tag{14}
 \end{aligned}$$

where

$$\phi_n(y, y') = \frac{(\omega - 1 - 2n)(b_n)_n}{n! \Gamma(b_n)} (\theta^2 y y')^{-n} M(-n, b_n, \theta y) M(-n, b_n, \theta y')$$

and

$$\phi_\nu(y, y') = \frac{1}{2\pi} \frac{\Gamma(a_\nu)\Gamma(a_{-\nu})}{|\Gamma(2i\nu)|^2} (\theta^2 y y')^{i\nu} U(a_\nu, b_\nu, \theta y) U(a_\nu, b_\nu, \theta y')$$

now with

$$s_n = n(n + 1 - \omega), \quad b_n = \omega - 2n, \quad a_\nu = \frac{1}{2}(1 - \omega) + i\nu, \quad b_\nu = 1 + 2i\nu$$

We are also using the convention that  $\sum_n^m(\dots) = 0$  if  $m < n$ .

Recall we suppose  $\omega > 1$ , so the stationary density exists. Since  $\int \Psi(y') dy' = 1$ , the remaining terms must have a zero  $(y')$ -integral. Indeed this is true because,

$$(i) \quad \int (y')^{-3/2+\omega/2+i\nu} e^{-y'} U(a_\nu, b_\nu, y') dy' = 0,$$

which follows from taking the parameters  $\psi \rightarrow 0$  and  $\zeta = 1$  in the integral (29) below, and

$$(ii) \quad \int (y')^{\omega-2-n} e^{-y'} M(-n, \omega - 2n, y') dy' = 0, \quad \text{for } n = 1, 2, \dots, \lfloor \omega - 1 \rfloor.$$

Here (ii) follows from the relation

$$\int (y')^{\omega-2-n} e^{-y'} M(-n, \omega - 2n, y') dy' = \frac{(\omega - 2n)}{(\omega - 1 - n) \Gamma(1 - n)}, \quad (\omega > 1 + n), \quad (15)$$

which we found from Mathematica, where  $n$  is arbitrary real, and then specializing to  $n = 1, 2, \dots, \lfloor \omega - 1 \rfloor$ .  $\square$

**Remarks for the sub-case:**  $0 \leq \omega < 1$ . Norm preservation for this sub-case is best shown with the fundamental transform  $H$  developed later in Sec. 5. With that, the property amounts to showing that  $H(T, y; z = 0) = 1$ . But, referring to (35), it is easy to see that  $h(y; z = 0) = 1$  and then  $H(T, y; z = 0) = 1$  is immediate from (33)-(34).

### 2.5.3 The SABR model limit: no drifts

Drop the drifts in (1) and you have the (lognormal) SABR model. Then (10) yields previously known SABR results. Details are found in Appendix B.



### 3 Risk-neutral evolution

Given a P-measure diffusion, to avoid arbitrage opportunities, options must be valued under an equivalent Q-measure diffusion. The usual short-hand trick to finding it are Girsanov substitutions:  $dB_t \rightarrow dB_t^* - \lambda_t^e$  and  $dW_t \rightarrow dW_t^* - \lambda_t^v$  in (1). Here  $(B_t^*, W_t^*)$  are Q-Brownian motions and  $(\lambda_t^e, \lambda_t^v)$  are, respectively, market prices of equity and volatility risk.

We assume a world with a constant “cost-of-carry”  $b = r - q$ , where  $r$  is a short-term interest rate, and  $q$  is a constant dividend yield thrown off by the asset. Then, given our parametrization in (1), the absence of arbitrage requires

$$\lambda_t^e = \frac{\alpha + \beta\sigma_t^2 - (r - q)}{\sigma_t}$$

In principle, any functional choice  $\lambda_t^v = \lambda^v(t, S_t, \sigma_t)$  that preserves the inaccessibility of all the spatial boundaries will bring closure to the model and satisfy the “no-arbitrage” principle: P-Q equivalence as measures. In practice, one wants to preserve ‘closed formness’. Indeed, a convention in financial modelling (although not required by the general theory) is to arrange both the P and Q evolutions to have similar parameterizations. This allows a successful solution method for one to work for the other. In this spirit, our simple choice here takes  $\lambda^v$  a constant. With that,

$$\text{under Q: } \begin{cases} dS_t = (r - q)S_t dt + \sigma_t S_t dB_t^*, \\ d\sigma_t = \sigma_t(\omega_Q - \theta \sigma_t) dt + \xi \sigma_t dW_t^*, \\ dB_t^* dW_t^* = \rho dt, \end{cases} \quad (16)$$

where  $\omega_Q = \omega - \lambda^v \xi$ , and now (1) and (16) together complete the model.

To simplify the notations, let us agree that all the evolutions and Brownian motions in this section are ‘under Q’. Then we have, equivalently, the Q-model:

$$\begin{cases} dX_t = (r - q - \frac{1}{2} Y_t^2) dt + Y_t dB_t, \\ dY_t = (\omega_Q Y_t - \theta Y_t^2) dt + \xi Y_t dW_t, \\ dB_t dW_t = \rho dt. \end{cases} \quad (17)$$

### 3.1 The issue of martingality

The XGBM model nests the lognormal SABR model as a special case: see (75) in Appendix B. Recall that, under the lognormal SABR model, the stock price process can suffer ‘loss of martingality’ due to the correlation parameter  $\rho$ . Specifically,  $S_t$  is: (i) a true martingale when  $-1 \leq \rho \leq 0$ , and (ii) a strictly local martingale when  $0 < \rho \leq 1$ . Since every local martingale that is bounded from below is a supermartingale:  $\mathbb{E}_{S_0, \sigma_0} [S_t] < S_0$  (when  $\rho > 0$ ).

Indeed, when  $\rho > 0$ , I calculate explicitly in [6] the martingale defect. For the full XGBM model, correspondingly: when is the discounted stock price process  $\hat{S}_t := e^{(q-r)t} S_t$  a true martingale? Equivalently, fixing a forward settlement date  $T$ , when is the forward price process  $F_{t,T} = e^{(r-q)(T-t)} S_t$  a true martingale? Suppressing  $T$ , the evolution for that is:

$$\text{under Q: } \begin{cases} dF_t = \sigma_t F_t dB_t^*, \\ d\sigma_t = \sigma_t (\omega_Q - \theta \sigma_t) dt + \xi \sigma_t dW_t^*, \\ dB_t^* dW_t^* = \rho dt, \end{cases} \quad (18)$$

A prescription for answering this question is given in [5],[6] for the general stochastic volatility evolution  $d\sigma_t = b(\sigma_t) dt + a(\sigma_t) dW_t$ . To determine if this process is martingale-preserving (for the forward), introduce the *auxiliary* volatility process  $\{\hat{\sigma}_t\}$ :

$$d\hat{\sigma}_t = [b(\hat{\sigma}_t) + \rho \hat{\sigma}_t a(\hat{\sigma}_t)] dt + a(\hat{\sigma}_t) dW_t.$$

Then, the forward  $F_t$  suffers a loss of martingality if and only if the auxiliary process can ‘explode’; i.e., reach  $\hat{\sigma} = +\infty$  in finite time with strictly positive probability. From (18), for the case under consideration,

$$d\hat{\sigma}_t = (\omega_Q \hat{\sigma}_t - \delta \hat{\sigma}_t^2) dt + \xi \hat{\sigma}_t dW_t, \quad \text{where } \delta = \theta - \rho \xi.$$

Then, by applying the *Feller explosion criteria* (details in [5]), one can establish that  $\hat{\sigma}_t$  can explode if and only if  $\delta < 0$ ; i.e.,  $\rho > \theta/\xi$ .

Even better, when  $\rho > \theta/\xi$ , one can find the *martingale defect* by, equivalently, finding the *absorption-at-zero probability*  $A(x, t)$  for the inverse process  $X_t = 1/\hat{\sigma}_t$ . From Itô,

$$dX_t = (\alpha X_t + \delta) dt + \xi X_t dW_t, \quad \text{where } \alpha = \xi^2 - \omega_Q. \quad (19)$$

With  $\tau_0$  the first time the  $X$ -process hits zero,  $A(x, t)$  is defined by

$$A(x, t) = \mathbb{P}(X(\tau_0) \leq t | X_0 = x).$$

Then, the martingale defect is given by  $\mathbb{E}_{S_0, \sigma_0} [S_t/S_0] = 1 - A(1/\sigma_0, t)$ , with an explicit formula found in Appendix C.

In summary, the XGBM model, parametrized at (16) suffers a loss of martingality for the forward only when  $\rho$  is found in the interval  $\theta/\xi < \rho \leq 1$ . For (broad-based) equity applications, the condition is typically harmless: one will usually estimate both  $\rho < 0$  (negative option ‘skews’) and  $\theta > 0$  (volatility has a stationary density). But for other applications (possibly with positive option skews or negative  $\theta$ ’s), it is an issue to keep in mind.

## 4 Option valuation – Case 1: $\omega_Q \geq \xi^2/2$

Let  $q(t, x', y'|x, y)$  denote the XGBM transition density under the  $Q$ -evolution. From (11), with  $\alpha \rightarrow (r - q)$ ,  $\beta \rightarrow 0$ , and taking dummy  $z \rightarrow -z$ , we have

$$q(t, x', y'|x, y) = \int_{-\infty}^{\infty} e^{iz(x' - x - (r-q)t)} G\left(\frac{1}{2}\xi^2 t, y, y'; \tilde{\omega}, \theta_z^+, c_z^-\right) \frac{dz}{2\pi}, \quad (20)$$

$$\text{where } \tilde{\omega} = \frac{2\omega_Q}{\xi^2}, \quad \theta_z^+ = \frac{2}{\xi^2}(\theta + iz\rho\xi), \quad c_z^- = \frac{1}{\xi^2}(z^2 - iz). \quad (21)$$

Here  $G(t, y, y'; \omega, \theta, c)$  is again given at (10). Let  $V(x, y, T)$  denote the time-0 value of a Euro-style option with time- $T$  bounded payoff function  $w(x)$ . Then, since  $V$  is the time-0 discounted expected value of the payoff under the  $Q$ -evolution, we have generally

$$V(x, y, T) = \frac{e^{-rT}}{2\pi} \times \int_{-\infty}^{\infty} \int_0^{\infty} \int_{-\infty}^{\infty} e^{iz(x' - x - (r-q)T)} w(x') G\left(\frac{1}{2}\xi^2 T, y, y'; \tilde{\omega}, \theta_z^+, c_z^-\right) dz dy' dx'. \quad (22)$$

While (22) offers a quasi-analytic solution, it has an embarrassing number of integrations: 4(!), counting the integration for  $G$  itself. We'll eliminate two.

Proceeding formally, suppose it's legitimate to do the  $y'$  integral in (22) *first*. Then, *if the following integral exists*, define a *fundamental transform*

$$? \quad H(T, y; z) := \int_0^{\infty} G\left(\frac{1}{2}\xi^2 T, y, y'; \tilde{\omega}, \theta_z, c_z\right) dy', \quad z \in \mathcal{S}_1, \quad (23)$$

where  $\mathcal{S}_1$  is an analyticity strip for  $H$  in the complex  $z$ -plane. Note that we are now generalizing (22) by moving the  $z$ -integration off the real  $z$ -axis.

For options, our preferred strip for Fourier inversions is:  $0 < \Im z < 1$ . It can be shown that our preferred strip is contained within  $\mathcal{S}_1$  for XGBM because the model is (i) norm-preserving and (ii) martingale-preserving (under the mild restriction  $-1 \leq \rho \leq \min(1, \theta/\xi)$ ).<sup>2</sup>

We will show below that the question mark in front of (23) can be removed for Case 1. Next, in a familiar argument, define the (generalized) *payoff transform*

$$\hat{w}(z) = \int_{-\infty}^{\infty} e^{izx} w(x) dx, \quad z \in \mathcal{S}_w, \quad (24)$$

with  $z$  located in some other analyticity strip  $\mathcal{S}_w$ . We can always find a nice payoff such that these two horizontal strips intersect:  $\mathcal{S}_V = \mathcal{S}_1 \cap \mathcal{S}_w \neq \emptyset$ . Finally, by the arguments in my article “A Simple Option Formula for General Jump-diffusion and other Exponential Lévy Processes” (reprinted in [6]), (22) becomes

<sup>2</sup>To show that (i) and (ii) lead to analyticity in the preferred strip, see Th. 4.7 in [6].

$$V(x, y, T) = \frac{e^{-rT}}{2\pi} \int_{1c-\infty}^{1c+\infty} e^{-1z(x+(r-q)T)} H(T, y; z) \hat{w}(z) dz, \quad z \in \mathcal{S}_V. \quad (25)$$

In other words,  $1c$  is a point in the  $z$ -plane marking the intersection of a horizontal integration contour in  $\mathcal{S}_V$  with the imaginary  $z$ -axis. Again, we can arrange things so that we are working in the preferred strip:  $0 < c < 1$ . Reported numerics are found from versions of (25). For example, with  $x = \log S_0$ ,  $X = (r - q)T + \log S_0/K$  with strike price  $K$ , and  $c = \frac{1}{2}$ , all reported put option values  $P(x, y, T)$  are computed from:

$$P(x, y, T) = Ke^{-rT} \left( 1 - \int_{1c}^{1c+\infty} \Re \left\{ e^{-1zX} \frac{H(T, y; z)}{z^2 - 1z} \right\} \frac{dz}{\pi} \right). \quad (26)$$

**Removing the question mark in (23).** Recall that the SABR model is a special case of the XGBM model, with the transition density given at (77) in Appendix B. It turns out that, for the SABR model, the integral in (23) does *not* exist.

This problem was discussed in [6] (Sec. 8.13, pg. 407), but we will recap briefly here. For SABR, the existence of (23) amounts to integrating (77) from Appendix B with respect to  $y'$ , at fixed  $(\nu, z)$ . Extracting the few terms in (77) with  $y'$  dependence yields the integral

$$\int_0^\infty (y')^{-3/2} e^{-1z\rho y'/\xi} K_{1\nu}(\chi_z y') dy',$$

which does not exist because the integrand is not integrable as  $y' \downarrow 0$ .<sup>3</sup>

Now, for the SABR limit, there is no discrete spectral contribution to  $G$  in (10). The lesson from SABR is that, in the general XGBM case, problems may lie with integrating the continuous spectrum term. Indeed, extracting all the  $y'$  dependencies from the continuous spectrum term in (10), the corresponding XGBM integral is

$$(*) \quad \int_0^\infty (y')^{\tilde{\omega}/2-3/2} e^{-(\theta_z^+ + \gamma_z)y'} (y')^\nu U(a_\nu, b_\nu, R_z y') dy'.$$

$$\text{Recall } \tilde{\omega} = \frac{2\omega_Q}{\xi^2}, \quad \theta_z^+ = \frac{2}{\xi^2}(\theta + 1z\rho\xi), \quad c_z^- = \frac{1}{\xi^2}(z^2 - 1z),$$

$$\text{and so } \gamma_z = -\frac{1}{2} \left( \theta_z^+ - \sqrt{(\theta_z^+)^2 + 4c_z^-} \right), \quad R_z = \theta_z^+ + 2\gamma_z = \sqrt{(\theta_z^+)^2 + 4c_z^-}.$$

Now, first consider the integrand as  $y' \downarrow 0$ . As  $x \rightarrow 0$ ,  $U(a, b, x) \sim c_1 + c_2 x^{1-b}$ , where  $c_{1,2}$  are bounded constants independent of  $x$ . Since  $b_\nu = 1 + 2\nu$ ,

$$(y')^\nu U(a_\nu, b_\nu, R_z y') \sim c_1 (y')^\nu + c_2 (y')^{-\nu},$$

---

<sup>3</sup> $K_{1\nu}(y) \sim c_1 y^{-\nu} + c_2 y^\nu$ , as  $y \rightarrow 0$ , where  $c_{1,2}$  depend upon  $\nu$  but not  $z$ .

much like the SABR case with Bessel functions discussed in footnote 3. The exponential is harmless at small  $y'$ , so we see the crux of the matter is the term  $(y')^{\tilde{\omega}/2-3/2}$ , which is integrable iff<sup>4</sup>

$$\boxed{\tilde{\omega} \geq 1, \quad (\text{i.e., } \omega_Q \geq \frac{1}{2}\xi^2), \quad (\text{Case 1: integrability condition})} \quad (27)$$

When the integrability condition holds, so does (23). Recall we have seen this condition before at (12) in the P-model: there needed for the existence of a stationary limit of the stand-alone volatility process. In most financial applications (with calibrated parameters), the integrability condition will be satisfied. Thus, to borrow a characterization from physics, Case 1 is the “physical case”. Case 2 is the “unphysical case” (including SABR). Case 2 is, of course, still mathematically well-defined.

What about  $y' \rightarrow \infty$ ? Since

$$\theta_z^+ + \gamma_z = \frac{1}{2} \left( \theta_z^+ + \sqrt{(\theta_z^+)^2 + 4c_z^-} \right),$$

this term will have positive real part in the preferred  $z$ -plane strip. As the remaining integrand terms in (\*) have power law behavior as  $y' \rightarrow \infty$ , the net effect is exponential decay in  $y'$  at large  $y'$ , so all is well in that limit.

To summarize at this point, we have the following situation. In the risk-neutral model, when the integrability condition (27) holds, option values are given by (25), with  $H$  given by (23). If the integrability condition does *not* hold (Case 2), option values are *still* given by (25), but  $H(\cdot)$  is *not* given by (23). Instead, that integral needs to be regularized: see Sec. 5 for details. In this section, we now continue, assuming (27) holds.

**Option valuation – continued.** To perform the integration in (\*), use a formula from Slater ([9], (3.2.51)-(3.2.52)):

$$\begin{aligned} & \int_0^\infty e^{-st} t^{c-1} U(a, b, t) dt \\ &= \frac{\Gamma(c)\Gamma(1+c-b)}{\Gamma(1+a+c-b)} \times \begin{cases} F(c, 1+c-b, 1+a+c-b; 1-s), & |1-s| < 1, \\ s^{-c} F\left(a, c, 1+a+c-b; 1-\frac{1}{s}\right), & \Re s > \frac{1}{2}, \end{cases} \\ & \quad \text{for } \Re c > 0, \quad \Re b < \Re c + 1. \end{aligned} \quad (28)$$

Here  $F(a, b, c; z) = \sum_{n=0}^\infty \frac{(a)_n (b)_n}{(c)_n} \frac{z^n}{n!}$  is the Gauss hypergeometric function. Note that the two conditions on  $s$  above can overlap, allowing both integral relations to be true at the same time. Applying (28) to our problem (\*) above yields:

$$\begin{aligned} & \int_0^\infty (y')^{\tilde{\omega}/2-3/2+1\nu} e^{-(\theta_z^+ + \gamma_z)y'} U(a_\nu, b_\nu, R_z y') dy' \\ &= \frac{|\Gamma(c_\nu)|^2}{R_z^{c_\nu} \Gamma(\psi)} \times \begin{cases} F(c_\nu, c_\nu^*, \psi; 1 - \zeta_z), & |1 - \zeta_z| < 1, \\ s^{-c_\nu} F\left(a_\nu, c_\nu, \psi; 1 - \frac{1}{\zeta_z}\right), & \Re \zeta_z > \frac{1}{2}, \end{cases} \end{aligned}$$

<sup>4</sup>Integrability is clear when  $\tilde{\omega} > 1$ . The borderline case  $\tilde{\omega} = 1$  is not as immediate, but (29) below shows that (\*) also exists when  $\tilde{\omega} = 1$  as long as  $\nu > 0$ .

$$\text{where } a_\nu = \frac{1}{2}(1 - \tilde{\omega}) + \psi_z + \nu, \quad c_\nu = -\frac{1}{2} + \frac{1}{2}\tilde{\omega} + \nu, \quad \psi_z = \frac{\tilde{\omega}\gamma_z}{R_z}, \quad (29)$$

$$\text{and } \zeta_z = \frac{1}{2} \left( 1 + \frac{\theta_z^+}{\sqrt{(\theta_z^+)^2 + 4c_z^-}} \right). \quad (30)$$

Note  $c_\nu^* = -\frac{1}{2} + \frac{1}{2}\tilde{\omega} - \nu$  denotes the complex conjugate of  $c_\nu$  (since  $\tilde{\omega}$  is real). The integration conditions  $\Re c > 0$  and  $\Re b < \Re c + 1$  from Slater reduce to:  $\tilde{\omega} > 1$ . (Recall in fact  $\tilde{\omega} = 1$  is OK for Case 1 as long as  $\nu \neq 0$ ). The  $\zeta_z$ -value restrictions can be checked along any putative  $z$ -plane integration contour; I have found the  $|1 - \zeta_z| < 1$  formulas suffice for all the test examples of Sec. 7.

**The discrete term integration.** From (10) and (23), the discrete term in the spectral expansion requires

$$(**) \int_0^\infty (y')^{\tilde{\omega}-2+r_n} e^{-(\theta_z^+ + \gamma_z)y'} M(-n, b_n, R_z y') dy',$$

where  $r_n = -(n + \psi)$  and  $\psi$  is given at (29). The integral (\*\*) can be performed using another formula from Slater, (3.2.16):

$$\int_0^\infty e^{-st} t^{c-1} M(-n, b, kt) dt = \Gamma(c) s^{-c} F\left(-n, c, b; \frac{k}{s}\right), \quad (31)$$

for  $\Re c > 0$ ,  $\Re s > 0$ , and  $n = 0, 1, 2, \dots$

Note that, since  $n$  is an integer for our application,  $F(-n, c, b, z)$  is a terminating polynomial of  $O(z^n)$ . Thus,

$$\begin{aligned} \int_0^\infty (y')^{\tilde{\omega}-2+r_n} e^{-(\theta_z^+ + \gamma_z)y'} M(-n, b_n, R_z y') dy' \\ = \Gamma(c_n) (R_z \zeta_z)^{-c_n} F\left(-n, c_n, b_n; \frac{1}{\zeta_z}\right), \end{aligned}$$

where  $c_n = \tilde{\omega} - 1 + r_n$ ,  $b_n = \tilde{\omega} + 2r_n$ , and  $\zeta_z$  is defined at (30).

**Remarks.** Note that the last Slater integral (31) requires  $\Re c > 0$ , which translates to  $\Re c_n > 0$ . It can be seen that this condition is automatically satisfied here as follows. First,  $\Re c_n > 0$  is equivalent to  $\tilde{\omega} - 1 > (n + \Re \psi)$ . But, if  $s_n$  contributes to the discrete spectrum, then  $\tilde{\omega} - 1 > 2(n + \Re \psi)$  (see Appendix A or the sum cutoff in (32)). When this last inequality is satisfied, the l.h.s. will be positive. And certainly if  $A > B$  with  $A$  positive but otherwise arbitrary, then  $A > B/2$ .

## 4.1 Frequently used notations under risk-neutrality

Here we collect in one place notation we have introduced and will frequently refer to subsequently.

$$\begin{aligned}
\tilde{\omega} &= \frac{2\omega}{\xi^2}, & \theta_z^+ &= \frac{2}{\xi^2}(\theta + 1z\rho\xi), & c_z^- &= \frac{1}{\xi^2}(z^2 - 1z), \\
R_z &= \sqrt{(\theta_z^+)^2 + 4c_z^-}, & \gamma_z &= -\frac{1}{2}\theta_z^+ + \frac{1}{2}R_z, & \zeta_z &= \frac{1}{2}\left(1 + \frac{\theta_z^+}{R_z}\right), & \psi_z &= \frac{\tilde{\omega}\tilde{\gamma}_z}{R_z}, \\
a_\nu &= \frac{1}{2}(1 - \tilde{\omega}) + \psi_z + 1\nu, & b_\nu &= 1 + 21\nu, & c_\nu &= -\frac{1}{2} + \frac{1}{2}\tilde{\omega} + 1\nu, \\
r_n &= -(n + \psi_z), & s_n(z) &= (n + \psi_z)^2 + (1 - \tilde{\omega})(n + \psi_z), \\
b_n &= \tilde{\omega} + 2r_n, & c_n &= \tilde{\omega} - 1 + r_n.
\end{aligned}$$

Note that here and throughout, we frequently suppress  $z$ -dependencies to ease notations, as we have done with  $(a_\nu, r_n, b_n, c_n)$ .

## 4.2 Summary: fundamental transform for Case 1

Putting it all together, for  $\omega \geq \xi^2/2$ , we have the spectral representation:

$$\begin{aligned}
H(T, y; z) &= \int_0^\infty G(\tau, y, y'; \tilde{\omega}, \theta_z^+, c_z^-) dy' \\
&= e^{-\gamma_z y} \left\{ 1_{\{\frac{\tilde{\omega}-1}{2} > \Re\psi_z\}} \sum_{n=0}^{\lfloor (\tilde{\omega}-1)/2 - \Re\psi_z \rfloor} \phi_n(R_z y) e^{s_n(z)\tau} + \int_0^\infty \phi_\nu(R_z y) e^{-(\nu^2 + \frac{1}{4}(1-\tilde{\omega})^2)\tau} d\nu \right\}
\end{aligned} \tag{32}$$

where  $\tau = \frac{1}{2}\xi^2 T$ ,

$$\begin{aligned}
\phi_n(y) &= \frac{(\tilde{\omega} - 1 - 2n - 2\psi)(b_n)_n \Gamma(c_n)}{n! \Gamma(b_n)} \zeta_z^{-c_n} F\left(-n, c_n, b_n; \frac{1}{\zeta_z}\right) y^{r_n} M(-n, b_n, y), \\
\phi_\nu(y) &= \frac{1}{2\pi} \frac{\Gamma(a_\nu)\Gamma(a_\nu - \nu)|\Gamma(c_\nu)|^2}{|\Gamma(2i\nu)|^2 \Gamma(\psi_z)} y^{(1-\tilde{\omega})/2 + 1\nu} U(a_\nu, b_\nu, y) \\
&\quad \times \begin{cases} F(c_\nu, c_\nu^*, \psi_z; 1 - \zeta_z), & |1 - \zeta_z| < 1, \\ \zeta_z^{-c_\nu} F\left(a_\nu, c_\nu, \psi_z; 1 - \frac{1}{\zeta_z}\right), & \Re\zeta_z > \frac{1}{2}, \end{cases}
\end{aligned}$$

with other notations in Sec. 4.1. Again, some  $z$ -dependencies are suppressed.

## 5 Option valuation – Case 2: $0 \leq \omega_Q < \xi^2/2$

To handle this case, we'll adapt the method I used for the SABR model in [6]. Consider  $h(y)$ , a putative time-independent solution to the PDE in the top line of (9). Suppose  $h(y) \sim 1 + O(y^{1-\tilde{\omega}})$  as  $y \rightarrow 0$  and  $h(y)$  decays at large  $y$ . Note an initial condition plays no role in this time-independent problem. (With  $\theta \rightarrow \theta_z$  and  $c \rightarrow c_z$ , we write this solution as  $h(y; z)$ ). With that putative solution, the fundamental transform  $H(T, y; z)$  can be constructed as

$$H(T, y; z) = h(y; z) + H_{reg}(\tau, y; z), \quad (\tau = \frac{1}{2}\xi^2 T). \quad (33)$$

Here a *regularized* fundamental transform  $H_{reg}(\tau, y; z)$  is defined by

$$H_{reg}(\tau, y; z) := \int_0^\infty (1 - h(y'; z)) G(\tau, y, y'; \tilde{\omega}, \theta_z^+, c_z^-) dy', \quad z \in \mathcal{S}_1. \quad (34)$$

Let's review why this works. First, both terms on the r.h.s. of (33) manifestly satisfy the PDE associated to the fundamental transform – the top line of (9) again. Second, as  $T \rightarrow 0$ , because  $G(\dots)$  satisfies a Dirac mass initial condition, we have  $H_{reg}(0, y; z) = 1 - h(y; z)$ . Thus,  $H(0, y; z) = 1$ , which is the correct initial condition for the fundamental transform. Third, the integral in (34) exists because  $1 - h(y; z) \sim O(y^{1-\tilde{\omega}})$  as  $y \rightarrow 0$ , so the problematic integrand in (\*) is tamed by this new behavior. Finally,  $H(T, y; z)$  correctly decays at large  $y$  because both terms on the r.h.s. of (33) do.

Using the notations in Sec. 4.1 and the confluent hypergeometric  $U$ , I find

$$\boxed{h(y; z) = e^{-\gamma_z y} \frac{U(\psi_z, \tilde{\omega}, R_z y)}{U(\psi_z, \tilde{\omega}, 0)},} \quad (35)$$

which has the advertised  $y$ -behaviors. Now recall

$$U(a, b, z) = \frac{\Gamma(1-b)}{\Gamma(a-b+1)} M(a, b, z) + z^{1-b} \frac{\Gamma(b-1)}{\Gamma(a)} M(a-b+1, 2-b, z). \quad (36)$$

Since  $M$  has a Taylor expansion about  $z = 0$ , this implicitly defines coefficients  $(A_n, B_n)$  such that

$$h(y; z) = \sum_{n=0}^{\infty} A_n(z) (R_z y)^n + (R_z y)^{1-\tilde{\omega}} \sum_{n=0}^{\infty} B_n(z) (R_z y)^n.$$

I find (again using the Gauss hypergeometric function  $F(a, b, c; z)$ ) that

$$\begin{aligned} A_n(z) &= f_n(\psi_z, \tilde{\omega}, \zeta_z - 1), \\ B_n(z) &= \frac{\Gamma(\tilde{\omega} - 1)\Gamma(\psi_z - \tilde{\omega} + 1)}{\Gamma(1 - \tilde{\omega})\Gamma(\psi_z)} f_n(\psi_z - \tilde{\omega} + 1, 2 - \tilde{\omega}, \zeta_z - 1), \quad \text{where} \\ f_n(a, b, c) &= c^n \frac{F(a, -n, b; -\frac{1}{c})}{\Gamma(1+n)}. \end{aligned}$$



Note that, since  $f_0 = 1$ , the first sum of  $h$  is  $1 + O(y)$  and the second sum is  $O(y^{1-\tilde{\omega}})$ ; since  $\tilde{\omega} < 1$ , the net effect is  $h(y) \sim 1 + O(y^{1-\tilde{\omega}})$ , as promised.

The term-by-term integrals that are now needed in (34) can be done by the previously given formulas from Slater. The net result is that the previously introduced  $\phi_\nu(y)$  (for Case 1) generalizes to  $\phi_{\nu,n}(y)$  where

$$\begin{aligned} \phi_{\nu,n}(y) = & \frac{1}{2\pi} \frac{\Gamma(a_\nu)\Gamma(a_{-\nu})|\Gamma(c_{\nu,n})|^2}{|\Gamma(2i\nu)|^2 \Gamma(\psi_z)} y^{(1-\tilde{\omega})/2+i\nu} U(a_\nu, b_\nu, y) \\ & \times \begin{cases} F(c_{\nu,n}, c_{\nu,n}^*, \psi_z + n; 1 - \zeta_z), & |1 - \zeta_z| < 1, \\ (\zeta_z)^{-c_{\nu,n}} F\left(a_\nu, c_{\nu,n}, \psi_z + n; 1 - \frac{1}{\zeta_z}\right), & \Re \zeta_z > \frac{1}{2}, \end{cases} \end{aligned}$$

In addition, we need to introduce the new function  $\psi_{\nu,n}(y)$  where

$$\begin{aligned} \psi_{\nu,n}(y) = & \frac{1}{2\pi} \frac{\Gamma(a_\nu)\Gamma(a_{-\nu})|\Gamma(d_{\nu,n})|^2}{|\Gamma(2i\nu)|^2 \Gamma(1 - \tilde{\omega} + n + \psi_z)} y^{(1-\tilde{\omega})/2+i\nu} U(a_\nu, b_\nu, y) \\ & \times \begin{cases} F(d_{\nu,n}, d_{\nu,n}^*, 1 - \tilde{\omega} + \psi_z + n; 1 - \zeta_z), & |1 - \zeta_z| < 1, \\ (\zeta_z)^{-d_{\nu,n}} F\left(a_\nu, d_{\nu,n}, 1 - \tilde{\omega} + \psi_z + n; 1 - \frac{1}{\zeta_z}\right), & \Re \zeta_z > \frac{1}{2}, \end{cases} \end{aligned}$$

These functions use the new notations:

$$\begin{aligned} c_{\nu,n} &= n - \frac{1}{2} + \frac{1}{2}\tilde{\omega} + i\nu, \quad (n \geq 1) \\ d_{\nu,n} &= n + \frac{1}{2} - \frac{1}{2}\tilde{\omega} + i\nu, \quad (n \geq 0). \end{aligned}$$

From these, form

$$\kappa(y; z) := \sum_{n=1}^{\infty} A_n(z) \phi_{\nu,n}(y) + \sum_{n=0}^{\infty} B_n(z) \psi_{\nu,n}(y) \quad (37)$$

and obtain finally, for Case 2,

$$\boxed{H(T, y; z) = h(y; z) - e^{-\gamma zy} \int_0^\infty \kappa_\nu(R_z y; z) e^{-(\nu^2 + \frac{1}{4}(1-\tilde{\omega}^2))\tau} d\nu.} \quad (38)$$

Don't forget that  $\tau = \frac{1}{2}\xi^2 T$  – both here and in (32). Equation (38) is the Case 2 replacement for (32); option values are computed from this new  $H$  using the previous (25) and (26).

## 6 Small and large time asymptotics

By ‘time’, we refer to the time-to-option-expiration  $T$ .

### 6.1 Small $T$

For small  $T$ , option prices at strike  $K$  tend to their parity values, and the implied volatility smile,  $\sigma_{imp}(T, K, S_0, \sigma_0)$ , tends to a non-trivial limit. Indeed, it is well-known that the limiting asymptotic smile in general SV models does not depend upon the diffusion drifts; it is solely determined by the variance-covariance system. In our case, that system is (75), which is the (lognormal) SABR model. The asymptotic smile formula for that one is well-known. The version I like is<sup>5</sup>

$$\sigma_0^{imp} := \lim_{T \rightarrow 0} \sigma_{imp}(T, K, S_0, \sigma_0) = \frac{z \sigma_0}{F(z)}, \quad \text{where } z = \left( \frac{2\xi}{\sigma_0} \right) \log \frac{S_0}{K}, \quad (39)$$

$$\text{and } F(z) = 2 \log \left\{ \frac{z/2 - \rho + \sqrt{1 - \rho z + z^2/4}}{1 - \rho} \right\}.$$

### 6.2 Large $T$

The large  $T$  option behavior is determined from the large  $T$  behavior of the fundamental transform  $H(T, \sigma; z)$ .

**Case 1:**  $\tilde{\omega} \geq 1$ . In this case, following the method in [5] (Ch. 6), one looks for the behavior (as  $T$  grows large)  $H(T, \sigma; z) \sim e^{-\lambda_0(z)T} u_0(\sigma; z)$  in the spectral expansion (32). When there is a discrete component in that expansion, then  $\lambda_0$  is the principal eigenvalue. When there is only a continuous spectrum, but still real  $\lambda_0 > 0$ , a better nomenclature for  $\lambda_0$  (borrowing from physics) might be be ‘mass gap’. In any event, we define  $\lambda_0$  by

$$\lambda_0(z) := \lim_{T \rightarrow \infty} -\frac{1}{T} \log H(T, \sigma; z).$$

Tentatively, assume the parameters are such that there is indeed a discrete spectrum, and identify  $\lambda_0(z)$  from the leading term of that. Using the notation associated to (32), one has

$$\lambda_0(z) = -\frac{1}{2}\xi^2 s_0(z) = -\frac{1}{2}\xi^2 [\psi^2(z) + (1 - \tilde{\omega})\psi(z)],$$

$$\text{where } \psi(z) = \frac{1}{2}\tilde{\omega} \left\{ 1 - \frac{(\theta + 1z\rho\xi)}{\sqrt{(\theta + 1z\rho\xi)^2 + (z^2 - 1z)\xi^2}} \right\}.$$

Then, the prescription in the cited reference is to look for a saddle point  $z^* = 1y^*$  in the complex  $z$ -plane along the purely imaginary axis (so  $y^*$  is real).

<sup>5</sup>I am copying in (39) from eq. (12.33) in [6] (Ch. 12). It is easily shown to be equivalent to other SABR model sources. For example, to show it is equivalent to (8.32) in [8], identify my  $z$  with  $-(2\nu q/\alpha)$  in Paulot and apply some routine algebra.

The saddle point is a solution to  $\lambda'_0(z) = 0$ , where the prime indicates the  $z$ -derivative. Having found that, the asymptotic  $T \rightarrow \infty$  option implied volatility  $V_\infty^{imp} = (\sigma_\infty^{imp})^2$  is given by the very simple relation

$$\boxed{V_\infty^{imp} = 8\lambda_0(z^*)}. \quad (40)$$

With  $\psi^* := \psi(\mathbf{1}y^*)$ , it's easy to find

$$y^* = \frac{\theta}{2\theta - \rho\xi} \quad \Rightarrow \quad \psi^* = \frac{\tilde{\omega}}{2} \{1 - \zeta\}. \quad (41)$$

$$\text{defining } \zeta := \frac{1}{(1 + \frac{\xi^2}{4\theta(\theta - \rho\xi)})^{1/2}}, \quad (\theta > \rho\xi).$$

Notice that we work in the ‘‘martingale-preserving’’ regime (recall Sec. 3.1), where  $-1 \leq \rho \leq (\theta/\xi)$ . Since we assume throughout that  $\theta \geq 0$ , in that regime  $\zeta \in [0, 1)$  and  $y^* \in [0, 1]$ , which is the preferred (and guaranteed) analyticity strip for  $H$ . Thus, we have found that *when  $\tilde{\omega}$  is such that a discrete spectrum exists*, then

$$\lambda_0^* := \lambda_0(z^*) = \frac{1}{2}\xi^2 [(\tilde{\omega} - 1)\psi^* - (\psi^*)^2],$$

$$\text{and } \sigma_\infty^{imp} = 2\xi\sqrt{(\tilde{\omega} - 1)\psi^* - (\psi^*)^2},$$

where  $\psi^*$  is given by (41). But, what is the criterion for a discrete spectrum to exist? From (32), and since  $\psi^*$  is real, a discrete spectrum exists when

$$\tilde{\omega} \geq 1 + 2\psi^* = 1 + \tilde{\omega}(1 - \zeta) \quad \Rightarrow \quad \tilde{\omega} \geq \frac{1}{\zeta}.$$

Now, since we are discussing Case 1, which has  $\tilde{\omega} \geq 1$ , the remaining sub-case to be addressed here is  $1 \leq \tilde{\omega} < (1/\zeta)$ . Since there is no discrete spectrum, only the continuous spectrum term contributes. One reads off from (32) that

$$H(T, \sigma; z) \sim e^{-(1-\tilde{\omega})^2\xi^2 T/8} u_0(\sigma; z);$$

$$\text{i.e., the mass gap } \lambda_0^* = \frac{1}{8}\xi^2(\tilde{\omega} - 1)^2, \quad (1 \leq \tilde{\omega} < \frac{1}{\zeta}),$$

with some  $u_0$  whose specific form doesn't matter for our purpose. Let's introduce the notation  $\tilde{\omega}_c := 1/\zeta$ , which marks the critical value of  $\tilde{\omega}$  such that a discrete spectrum emerges. To summarize, we've found under Case 1 (and the martingale-preserving regime) that the principal eigenvalue/mass gap is:

$$\boxed{\lambda^*(\tilde{\omega}) = \frac{1}{2}\xi^2 \begin{cases} (\tilde{\omega} - 1)\psi^*(\tilde{\omega}) - (\psi^*(\tilde{\omega}))^2, & \tilde{\omega}_c \leq \tilde{\omega} < \infty, \\ \frac{1}{4}(\tilde{\omega} - 1)^2, & 1 \leq \tilde{\omega} < \tilde{\omega}_c, \end{cases} \quad (42)}$$

where  $\tilde{\omega}_c = \frac{1}{\zeta}$ ,  $\psi^*(\tilde{\omega}) = \frac{\tilde{\omega}}{2} \{1 - \zeta\}$ , and  $\zeta = \frac{1}{(1 + \frac{\xi^2}{4\theta(\theta - \rho\xi)})^{1/2}}$ .

**Smoothness.** Notice that  $\psi^*(\tilde{\omega}_c) = (1 - \zeta)/(2\zeta) = \frac{1}{2}(\tilde{\omega}_c - 1)$ . Thus

$$(\tilde{\omega}_c - 1)\psi^*(\tilde{\omega}_c) - (\psi^*(\tilde{\omega}_c))^2 = \frac{1}{4}(\tilde{\omega}_c - 1)^2,$$

which shows that  $\lambda^*(\tilde{\omega})$  of (42) is continuous at  $\omega = \tilde{\omega}_c$ . By differentiating, it is easy to see that  $d\lambda^*(\tilde{\omega})/d\tilde{\omega}$  is also continuous at  $\omega = \tilde{\omega}_c$ . In other words  $\lambda^*(\tilde{\omega})$  is *smooth*, in the sense of being continuously differentiable, throughout the Case 1 regime:  $1 \leq \tilde{\omega} < \infty$ .

**Examples.** With  $\omega = \xi = 1$  and  $\rho = 0$ , then  $\tilde{\omega} = 2$ ,  $\psi^* = 0.007722$ , and  $\sigma_\infty^{imp} = 0.1751$ . Or, with  $\omega = \xi = 1$  and  $\rho = -0.75$ , then  $\psi^* = 0.006515$ , and  $\sigma_\infty^{imp} = 0.1609$ . This is how the  $T = \infty$  entries in Table 1 were found.

**Case 2.** For simplicity, suppose no cost-of-carry parameters, so  $r = q = 0$ . As  $T$  gets large under Case 2 the fundamental transform  $H$  does not decay, but instead has a non-trivial, but relatively simple limit:  $H(T, \sigma_0; z) \sim H_\infty(z, \sigma_0)$ . From (26):

$$P_\infty(S_0, \sigma_0; K) = K \left[ 1 - \frac{1}{2\pi} \int_\Gamma e^{-izX} \frac{H_\infty(z, \sigma_0)}{z^2 - iz} dz \right]. \quad (43)$$

Here the contour  $\Gamma$  is defined by  $0 < \Im z < 1$ , and  $X = \log(S_0/K)$ . Note that  $H_\infty(z, y)$  is not a new function in our development; indeed,  $H_\infty(z, y) = h(y; z)$ , where the r.h.s. was found previously at (35). Hence,

$$H_\infty(z, \sigma_0) = e^{-\gamma z \sigma_0} \times \begin{cases} \frac{U(\psi_z, \tilde{\omega}, R_z \sigma_0)}{U(\psi_z, \tilde{\omega}, 0)}, & 0 < \tilde{\omega} \leq 1, \\ 1, & \tilde{\omega} = 0, \end{cases} \quad (44)$$

and recall Sec. 4.1 for other notations.<sup>6</sup>

Numerical examples using (43-44) are found in the  $T = \infty$  entry in Table 2. A similar discussion for the SABR model is found in [6] (Sec. 8.12.1).

---

<sup>6</sup>The case  $\tilde{\omega} = 0$  most easily follows by seeking a stationary solution  $h(y; z)$  to the top line of (9) with  $\omega = 0$ . One easily find  $h(y; z) = e^{-\gamma z y}$ . Alternatively, it can be checked by proving  $\lim_{b \rightarrow 0} U(a, b, z)/U(a, b, 0) = 1$ .

## 7 Numerical examples for option prices

Formulas are implemented in Mathematica; prices use (26). All required special functions are built in. We have a double integration. Additional complications that must be handled are now discussed.

### Implementation notes: Case 1.

For the ‘physical’ Case 1 ( $\omega \geq \xi^2/2$ ), we have a double integration using confluent hypergeometric functions with complex arguments. Results are not immediate. For example, with my choices for cutoffs and Precision parameters, option prices are found in 0.5-2 minutes on my desktop machine.

The main complication in this case is that, prior to the Fourier integration over  $z$ , one must identify the transition points (if any: see Appendix A) where the discrete and continuous parts of  $H$  are discontinuous. In Mathematica, I wrote a module `GetAllTransitionPts[.]`, which returns a list of such points. As I integrate in the  $z$ -plane over the line  $z = 1/2 + x$  for  $x \in [0, x_{max}]$ , the list only includes transition points in that (finite) interval. Now, in Mathematica, when integrating using `NIntegrate[.]` and typical defaults, the integration is adaptive and you don’t know in advance what points will be sampled. In the function returning the integrand, I first determine if each sample point  $x$  is near any transition point  $x^*$ , nearness meaning  $x \in (x^* - \epsilon, x^* + \epsilon)$ , where  $\epsilon > 0$  is small. If not near, I just return the ‘normal’ integrand. If near, I return the linearly interpolated  $H$ -value, using the endpoint values at  $x_1 = x^* - \epsilon$  and  $x_2 = x^* + \epsilon$ . This keeps  $H$  continuous, while avoiding troublesome evaluations of the discontinuous components too close to their transition points.

### Implementation notes: Case 2.

For the unphysical Case II ( $\omega < \xi^2/2$ ), the good news is that there are no discontinuity points. The bad news is that the integrand requires the infinite sum at (37). I truncate that sum, and make some use of Mathematica’s `Parallelize`. This case is really computationally tedious: results can take a half-hour or more.

### Examples.

As a first example, see Tables 1 and 2 for Cases 1 and 2 respectively. Table 3 shows additional at-the-money implied volatilities at larger  $T$ , the easiest regime for spectral solutions. There is good convergence to the exact analytic results at  $T = \infty$ , found in Sec. 6.2. Table 3 results are plotted Fig. 4.

Various results were spot-checked for consistency with Monte Carlos. As a stronger check, Table 4 shows some comparisons and good agreement with option values from a PDE solver.<sup>7</sup>

---

<sup>7</sup>The PDE solver was developed by Y. Papadopoulos, who provisionally extended the method in [7] to the XGBM model (private communication).

| T        | $(\omega = 1, \rho = 0)$ |                | $(\omega = 1, \rho = -0.75)$ |                | $(\omega = 2, \rho = -0.75)$ |                |
|----------|--------------------------|----------------|------------------------------|----------------|------------------------------|----------------|
|          | Option Price             | Implied Vol(%) | Option Price                 | Implied Vol(%) | Option Price                 | Implied Vol(%) |
| 0.25     | 4.126                    | 20.69          | 4.033                        | 20.23          | 4.543                        | 22.79          |
| 2        | 11.57                    | 20.57          | 10.78                        | 19.17          | 18.15                        | 32.46          |
| 20       | 30.97                    | 17.82          | 28.68                        | 16.44          | 61.26                        | 38.65          |
| 100      | 61.94                    | 17.54          | 58.03                        | 16.14          | 95.06                        | 39.30          |
| 500      | 94.98                    | 17.51          | 92.81                        | 16.10          | 99.999                       | 39.42          |
| $\infty$ | 100                      | 17.51          | 100                          | 16.09          | 100                          | 39.46          |

Table 1: **At-the-money option values for Case 1:**  $\omega \geq \xi^2/2$ . Other risk-neutral model parameters:  $S_0 = K = 100$ ,  $\sigma_0 = 0.20$ ,  $\xi = 1$ ,  $\theta = 4$ ,  $r = q = 0$ . Under the stationary density,  $\mathbb{E}[\sigma] = (0.125, 0.375)$  for  $\omega = (1, 2)$  respectively. The  $T = \infty$  Implied Vol entries are found from the square-root of (40).

| T        | $(\omega = \frac{1}{4}, \theta = 4)$ |                | $(\omega = \frac{1}{2}, \theta = 4)$ |                | $(\omega = 0, \theta = 0)$ |                |
|----------|--------------------------------------|----------------|--------------------------------------|----------------|----------------------------|----------------|
|          | Option Price                         | Implied Vol(%) | Option Price                         | Implied Vol(%) | Option Price               | Implied Vol(%) |
| 0.25     | 3.705                                | 18.58          | 3.809                                | 19.11          | 3.962                      | 19.87          |
| 2        | 7.287                                | 12.93          | 8.268                                | 14.68          | 10.35                      | 18.39          |
| 20       | 9.577                                | 5.38           | 13.56                                | 7.64           | 15.49                      | 8.74           |
| 100      | 9.756                                | 2.45           | 18.50                                | 4.68           | 15.554                     | 3.92           |
| 500      | 9.758                                | 1.10           | 25.82                                | 2.95           | 15.554                     | 1.75           |
| $\infty$ | 9.758                                | 0              | 100                                  | 0              | 15.554                     | 0              |

Table 2: **At-the-money option values for Case 2:**  $\omega < \xi^2/2$ . Other risk-neutral model parameters:  $S_0 = K = 100$ ,  $\sigma_0 = 0.20$ ,  $\xi = 1$ ,  $\rho = -0.75$ ,  $r = q = 0$ . The middle column is technically a Case 1 edge case, but it was computed two ways with the same result: (i) using Case 1 code with  $\omega = 0.5$  and (ii) using Case 2 code with  $\omega = 0.49999$ . For (ii), the sums in (37) were truncated at  $n = 10$  terms. The  $T = \infty$  price entries are computed from (43).

| T        | Implied Volatility (decimal) |        |        |        |        |       |       |       |       |       |       |       |
|----------|------------------------------|--------|--------|--------|--------|-------|-------|-------|-------|-------|-------|-------|
|          | Case 2                       |        |        |        | Case 1 |       |       |       |       |       |       |       |
|          | $\omega = 0.1$               | 0.2    | 0.3    | 0.4    | 0.5    | 0.6   | 0.7   | 0.8   | 0.9   | 1.0   | 1.1   | 1.2   |
| 10       | 0.1672                       | 0.2044 | 0.2518 | 0.3105 | 0.381  | 0.465 | 0.560 | 0.667 | 0.783 | 0.908 | 1.041 | 1.180 |
| 50       | 0.0813                       | 0.1070 | 0.1470 | 0.2080 | 0.294  | 0.405 | 0.537 | 0.683 | 0.840 | 1.004 | 1.172 | 1.344 |
| 250      | 0.0364                       | 0.0481 | 0.0678 | 0.1061 | 0.184  | 0.311 | 0.469 | 0.642 | 0.822 | 1.007 | 1.192 | 1.376 |
| $\infty$ | 0                            | 0      | 0      | 0      | 0      | 0.2   | 0.4   | 0.6   | 0.8   | 1.0   | 1.196 | 1.386 |

Table 3: **Large  $T$  behavior of the Implied Volatility.** Other risk-neutral model parameters:  $S_0 = K = 100$ ,  $\sigma_0 = 0.20$ ,  $\theta = 1/\sqrt{12}$ ,  $\xi = 1$ ,  $\rho = 0$ ,  $r = q = 0$ . The  $T = \infty$  entries are computed from the exact relations in Sec. 6.2. The data are plotted in Fig. 4.

| Implied Volatility at Various Strikes |        |        |        |        |
|---------------------------------------|--------|--------|--------|--------|
| Strike                                | Case A |        | Case B |        |
|                                       | PDE    | Exact  | PDE    | Exact  |
| 3400                                  | 0.6384 | 0.6384 |        |        |
| 3600                                  | 0.5854 | 0.5854 | 0.2813 | 0.2812 |
| 3800                                  | 0.5322 | 0.5322 | 0.2765 | 0.2765 |
| 4000                                  | 0.4787 | 0.4787 | 0.2719 | 0.2719 |
| 4200                                  | 0.4252 | 0.4252 | 0.2675 | 0.2676 |
| 4400                                  | 0.3742 | 0.3742 | 0.2634 | 0.2635 |
| 4600                                  | 0.3344 | 0.3344 | 0.2594 | 0.2595 |
| 4800                                  | 0.3196 | 0.3196 | 0.2557 | 0.2558 |
| 5000                                  | 0.3263 | 0.3263 | 0.2522 | 0.2524 |
| 5200                                  | 0.3420 | 0.3420 | 0.2490 | 0.2492 |
| 5400                                  | 0.3604 | 0.3604 | 0.2462 | 0.2463 |
| 5600                                  | 0.3792 | 0.3792 | 0.2437 | 0.2437 |

Table 4: **Numerical check: PDE vs. (quasi) exact solutions.** Table entries show the implied volatility (decimal) for two cases. For Case A:  $T = \frac{14}{365}$ ,  $r = 0.0357$ . For Case B:  $T = \frac{714}{365}$ ,  $r = 0.0401$ . Common parameters:  $S_0 = 4468.17$ ,  $q = 0$ ,  $\sigma_0 = 0.365113$ ,  $\omega = 24.8424$ ,  $\theta = 63.2858$ ,  $\rho = -0.517545$ ,  $\xi = 5.33384$ . As  $2\omega/\xi^2 > 1$ , this is a Case 1 comparison. Parameters and PDE values come from an XGBM model calibration against a (July 5, 2002) DAX index option chain using software developed by Y. Papadopoulos (footnote 7). Exact values are implied vols using prices computed from (26).

## 8 Other applications: $P$ -model parameter estimation

Maximum likelihood estimation (MLE) is the preferred approach – feasible using the transition density at (11) with a volatility proxy for the  $y$ 's. Key are dimensionless ratios such as  $\sigma_i^2(\theta/\xi)^2(T_i - T_{i-1})$  and  $\sigma_i(\omega\theta/\xi^2)(T_i - T_{i-1})$ , where  $\sigma_i = \sigma(T_i)$ . If the data observations are such that these ratios are not particularly small, then a fast and efficient (say C/C++) implementation is likely needed. However, when the ratios  $\ll 1$ , as may be the case with daily or weekly observations, then small-time asymptotics for the transition density should be effective and the exact formulas can simply serve as checks. Results along these lines will be reported in another publication.



## References

- [1] Milton Abramowitz and Irene A. Stegun. *Handbook of Mathematical Functions*. Dover, 1972.
- [2] P. Christoffersen, K. Jacobs, and K. Mimouni. Volatility dynamics for the S&P500: Evidence from realized volatility, data returns, and option prices. *Review of Financial Studies*, 23(8):3141–3189, 2010.
- [3] Pierre Henry-Labordere. *Analysis, Geometry, and Modeling in Finance: Advanced Methods in Option Pricing*. Chapman & Hall/CRC, 2009.
- [4] Alan L. Lewis. Applications of eigenfunction expansions in continuous-time finance. *Math. Finance*, 8:349–383, 1998. reprinted in Lewis (2016).
- [5] Alan L. Lewis. *Option Valuation under Stochastic Volatility: with Mathematica Code*. Finance Press, Newport Beach, California, 2000.
- [6] Alan L. Lewis. *Option Valuation under Stochastic Volatility II: With Mathematica Code*. Finance Press, Newport Beach, California, 2016.
- [7] Y. A. Papadopoulos and A. L. Lewis. A first option calibration of the GARCH diffusion model by a PDE method. arXiv:1801.06141 [q-fin.CP], 2018.
- [8] Louis Paulot. Asymptotic Implied Volatility at the Second Order With Application to the SABR Model. Revised version published at arxiv.org, Oct 11 2010. arXiv:0906.0658v2 [q-fin.PR], also available in P.K. Friz et al. (editors), ‘Large Deviations and Asymptotic Methods In Finance’, Springer 2015.
- [9] L.J. Slater. *Confluent Hypergeometric Functions*. Cambridge University Press, 1960.
- [10] M. Tegner and R. Poulsen. Volatility is log-normal – but not for the reason you think. *risks*, 6(2), 2018.

## 9 Appendix A – Proof of Theorem 1

The goal is to solve problem (9) for  $G(\tau, y, y')$ . With  $\Re s > 0$ , the Laplace transform  $\hat{G}(s, y, y') = \int e^{-s\tau} G(\tau, y, y') d\tau$  exists and solves

$$y^2 \hat{G}_{yy} + (\omega y - \theta y^2) \hat{G}_y - (s + cy^2) \hat{G} = -\delta(y - y'), \quad (y \in \mathbf{R}_+). \quad (45)$$

The associated homogeneous ODE

$$y^2 u'' + (\omega y - \theta y^2) u' - (s + cy^2) u = 0 \quad (46)$$

is converted to Kummer's differential equation in two steps. First, suppressing the dependence on  $(s, y')$ , let  $u(y) = e^{-\gamma y} y^r f(y)$ , choosing

$$\gamma = -\frac{1}{2}(\theta - \sqrt{\theta^2 + 4c}) \quad \text{and} \quad r = r_s = \frac{1}{2}(1 - \omega) + \frac{1}{2}\sqrt{(1 - \omega)^2 + 4s}. \quad (47)$$

This yields the ODE

$$y f'' + [(2r + \omega) - (2\gamma + \theta)y] f' - [r(2\gamma + \theta) + \omega\gamma] f = 0.$$

Second, let  $f(y) = w(x)$ , where  $x = Ry$ , choosing

$$R = \theta + 2\gamma = \sqrt{\theta^2 + 4c}. \quad (48)$$

With that,  $w(x)$  solves Kummer's differential equation

$$xw_{xx} + (b - x)w_x - aw = 0, \quad \text{with } b = b_s = \omega + 2r, \quad \text{and } a = a_s = r + \frac{\omega\gamma}{R}.$$

Note that in the case of real coefficients  $(\theta, c)$  with  $c > 0$ , we have both  $\gamma > 0$  and  $R > 0$ , regardless of the sign of  $\theta$ . To construct  $\hat{G}$ , we need solutions to Kummer's equation that are relatively small as  $x \rightarrow 0$  and  $x \rightarrow +\infty$  respectively. Suitable choices here are the confluent hypergeometric functions  $M(a, b, x)$  and  $U(a, b, x)$ . We denote the associated solutions to (46) as  $\xi(y, s)$  and  $\eta(y, s)$ . Using the above notations,

$$\xi(y, s) = e^{-\gamma y} (Ry)^r M(a, b, Ry) \quad \text{and} \quad \eta(y, s) = e^{-\gamma y} (Ry)^r U(a, b, Ry). \quad (49)$$

In terms of those, the solution to (45) has the well-known form:

$$\hat{G}(s, y, y') = \frac{-1}{(y')^2 W(y', s)} \begin{cases} \xi(y, s) \eta(y', s), & 0 \leq y \leq y', \\ \xi(y', s) \eta(y, s), & y' \leq y \leq \infty, \end{cases} \quad (50)$$

where  $W(y, s) := \xi \eta_y - \eta \xi_y$  is the Wronskian of  $(\xi, \eta)$ . With that, a first solution for the Green function  $G(\tau, y, y')$  is given by the Bromwich Laplace inversion

$$G(\tau, y, y') = \int_{\Gamma} \frac{ds}{2\pi i} e^{s\tau} \hat{G}(s, y, y'), \quad (51)$$

where  $\Gamma$  is a vertical line in the complex  $s$ -plane to the right of any singularities. As  $G(\tau, y, y')$  is a probability transition density, bounded on  $\tau > 0$ , then  $\hat{G}(s, y, y') = \int e^{-s\tau} G(\tau, y, y') d\tau$  is regular for all  $\Re s > 0$ . Thus, any vertical contour to the right of  $s = 0$  suffices for  $\Gamma$ : see Fig. 1.

Using Wronskians found in [1], we find

$$W(y, s) = -\frac{\Gamma(b_s)}{\Gamma(a_s)} R(Ry)^{-\omega} e^{\theta y} \quad (52)$$

Summarizing at this point, we have

First solution (Auxiliary Green function by Bromwich inversion):

$$\begin{aligned}
G(\tau, y, y') &= \int_{\Gamma} \frac{ds}{2\pi i} e^{s\tau} \hat{G}(s, y, y'), \text{ where } \Gamma \text{ is in Fig.1 and} \\
\hat{G}(s, y, y') &= \frac{\Gamma(a_s)}{\Gamma(b_s)} R^{b_s-1} y^{r_s} (y')^{r_s+\omega-2} e^{-\gamma y} e^{-(\gamma+\theta)y'} \\
&\quad \times \begin{cases} M(a_s, b_s, Ry) U(a_s, b_s, Ry'), & 0 \leq y \leq y', \\ M(a_s, b_s, Ry') U(a_s, b_s, Ry), & y' \leq y \leq \infty, \end{cases} \\
\text{using } R &= \sqrt{\theta^2 + 4c}, \quad \gamma = -\frac{1}{2}(\theta - \sqrt{\theta^2 + 4c}), \\
b_s &= 1 + \sqrt{(1-\omega)^2 + 4s}, \quad a_s = r_s + \frac{\omega\gamma}{R}, \\
\text{and } r_s &= \frac{1}{2}(1-\omega) + \frac{1}{2}\sqrt{(1-\omega)^2 + 4s}.
\end{aligned} \quad (53)$$

## 9.1 Spectral solution, Case 2

Case 2 is simpler in some respects, so a good place to begin. We construct the spectral solution from (53) via the Residue Theorem, extending the Bromwich contour to the closed path shown in Fig. 1. The precise nature of that path is explained below.

As one sees from (53),  $\hat{G}(s, y, y')$  is dependent upon the parameters  $b_s$  and  $r_s$ . Both have a (square-root) branch point singularity at  $s = s_c := -\frac{1}{4}(1-\omega)^2 \leq 0$ , using ‘c’ for ‘cut’. Regardless of the value of (real)  $\omega$ , this branch point is always present in the left half  $s$ -plane on the negative axis. We construct a branch cut along the negative  $s$  axis, extending from  $s_c$  to  $s = -\infty$ . Then, we integrate infinitesimally above and below the cut, along the contours  $C_1$  and  $C_2$  (Fig. 1).

Now  $\hat{G}$  may also have pole singularities *inside* the closed contour. Note the branch-cut is *outside*. However, it will be shown below that there are no such poles when  $0 \leq \omega < 1$ , our Case 2. It can also be shown that the contribution from the integrations along the curved quarter-circles of Fig. 1 vanish as these contour segments extend to  $|s| \rightarrow \infty$ . Hence, in that case,  $\hat{G}(s, y, y')$  is regular everywhere inside the closed contour of the figure: we have for Case 2, by the Residue Theorem,

$$G(\tau, y, y') = \int_{\Gamma} \frac{ds}{2\pi i} e^{s\tau} \hat{G}(s, y, y') = - \int_{C_1+C_2} \frac{ds}{2\pi i} e^{s\tau} \hat{G}(s, y, y'). \quad (54)$$

Now change integration variables from  $s$  to  $\nu$  by letting  $s = -\frac{1}{4}(1-\omega)^2 - \nu^2 \pm i\epsilon$  along  $C_1$  and  $C_2$  respectively. Then, as  $\epsilon \downarrow 0$ ,

$$\text{along } C_1 : \quad r_s \rightarrow r_\nu^+ := \frac{1}{2}(1-\omega) + i\nu, \quad b_s \rightarrow b_\nu^+ := 1 + 2i\nu, \quad a_s \rightarrow a_\nu^+ := r_\nu^+ + \psi_z,$$

abbreviating  $\psi_z = \omega\gamma_z/R_z$ . Importantly, while  $\psi_z$  generally depends upon the Fourier parameter  $z$ , it is *independent* of the Laplace parameter  $s$ . Similarly, as  $\epsilon \downarrow 0$ ,

$$\text{along } C_2 : \quad r_s \rightarrow r_\nu^- := \frac{1}{2}(1-\omega) - i\nu, \quad b_s \rightarrow b_\nu^- := 1 - 2i\nu, \quad a_s \rightarrow a_\nu^- := r_\nu^- + \psi_z.$$

Notice that, since  $a_\nu^\pm = \frac{1}{2}(1-\omega) \pm i\nu + \psi_z$ , we have for every fixed  $z$ ,

$$a_\nu^- + 2i\nu = a_\nu^+. \quad (55)$$

Suppressing dependencies on  $z$ , recall that

$$\eta(y, s) = e^{-\gamma y} (Ry)^{r_s} U(a_s, b_s, Ry).$$

Using the representation (36) and abbreviating  $\zeta := Ry$ , along  $C_1$ :

$$\begin{aligned} \eta(y, s) &\rightarrow \eta^+(y, \nu) := e^{-\gamma y} \zeta^{r_\nu^+} U(a_\nu^+, b_\nu^+, \zeta) \\ &= e^{-\gamma y} \zeta^{(1-\omega)/2 + i\nu} U(a_\nu^+, 1 + 2i\nu, \zeta) \\ &= e^{-\gamma y} \zeta^{(1-\omega)/2} \\ &\times \left[ \zeta^{i\nu} \frac{\Gamma(-2i\nu)}{\Gamma(a_\nu^+ - 2i\nu)} M(a_\nu^+, 1 + 2i\nu, \zeta) + \zeta^{-i\nu} \frac{\Gamma(2i\nu)}{\Gamma(a_\nu^+)} M(a_\nu^+ - 2i\nu, 1 - 2i\nu, \zeta) \right]. \end{aligned} \quad (56)$$

Similarly, along  $C_2$ :

$$\begin{aligned} \eta(y, s) &\rightarrow \eta^-(y, \nu) := e^{-\gamma y} \zeta^{r_\nu^-} U(a_\nu^-, b_\nu^-, \zeta) \\ &= e^{-\gamma y} \zeta^{(1-\omega)/2 - i\nu} U(a_\nu^-, 1 - 2i\nu, \zeta) \\ &= e^{-\gamma y} \zeta^{(1-\omega)/2} \\ &\times \left[ \zeta^{-i\nu} \frac{\Gamma(2i\nu)}{\Gamma(a_\nu^- + 2i\nu)} M(a_\nu^-, 1 - 2i\nu, \zeta) + \zeta^{i\nu} \frac{\Gamma(-2i\nu)}{\Gamma(a_\nu^-)} M(a_\nu^- + 2i\nu, 1 + 2i\nu, \zeta) \right]. \end{aligned}$$

Comparing, in light of (55), we have the key relation

$$\boxed{\eta^+(y, \nu) = \eta^-(y, \nu)}. \quad (57)$$

In other words,  $\eta(y, \cdot)$  is the same function of dummy integration variable  $\nu$  above and below the cut.<sup>8</sup> To see the implications of that, take the case where  $y \leq y'$ . Then, we have

<sup>8</sup>Another thing to notice is that, when the parameters  $(\omega, \theta, c)$  are *real*, then  $\eta(y, s)$  is also real along the cut. This follows because, under those assumptions, we have  $(a_\nu^+)^* = a_\nu^-$  and  $(b_\nu^+)^* = b_\nu^-$ , where the asterisk denotes complex conjugation. However,  $(a_\nu^+)^* \neq a_\nu^-$  generally in our application. To elaborate, that's because we have  $(\omega, \theta, c) \rightarrow (\omega, \theta_z, c_z)$  and, in general (with non-zero correlation)  $\theta_z = \frac{2}{\xi^2}(\theta + i z \rho \xi)$ , is not real along any Fourier inversion contour in the complex  $z$ -plane, although  $\theta$  itself is real. In turn, this causes  $\psi_z$  to not be real, which causes  $(a_\nu^+)^* \neq a_\nu^-$ .

$$\begin{aligned}
G(\tau, y, y') &= - \int_{C_1+C_2} e^{s\tau} \hat{G}(s, y, y') \frac{ds}{2\pi i} \\
&= (y')^{-2} e^{-(1-\omega)^2\tau/4} \int_0^\infty e^{-\nu^2\tau} \eta^+(y', \nu) \left[ \frac{\xi^+(y, \nu)}{W^+(y', \nu)} - \frac{\xi^-(y, \nu)}{W^-(y', \nu)} \right] \frac{\nu d\nu}{\pi i},
\end{aligned}$$

where

$$\begin{aligned}
\xi^+(y, \nu) &:= e^{-\gamma y} \zeta^{r_\nu^+} M(a_\nu^+, b_\nu^+, \zeta) \\
&= e^{-\gamma y} \zeta^{(1-\omega)/2} \zeta^{\nu} M(a_\nu^+, 1 + 2\nu, \zeta),
\end{aligned}$$

and

$$\begin{aligned}
\xi^-(y, \nu) &:= e^{-\gamma y} \zeta^{r_\nu^-} M(a_\nu^-, b_\nu^-, \zeta) \\
&= e^{-\gamma y} \zeta^{(1-\omega)/2} \zeta^{-\nu} M(a_\nu^-, 1 - 2\nu, \zeta).
\end{aligned}$$

And from (52),

$$W^\pm(y, \nu) = -R(Ry)^{-\omega} e^{\theta y} \frac{\Gamma(b_\nu^\pm)}{\Gamma(a_\nu^\pm)}.$$

Thus,

$$\begin{aligned}
G(\tau, y, y') &= -(y')^{-2} R^{-1}(Ry')^\omega e^{-\theta y'} e^{-\gamma y} \zeta^{(1-\omega)/2} e^{-(1-\omega)^2\tau/4} \\
&\times \int_0^\infty e^{-\nu^2\tau} \eta^+(y', \nu) \left[ \frac{\Gamma(a_\nu^+)}{\Gamma(b_\nu^+)} \zeta^{\nu} M(a_\nu^+, 1 + 2\nu, \zeta) - \frac{\Gamma(a_\nu^-)}{\Gamma(b_\nu^-)} \zeta^{-\nu} M(a_\nu^-, 1 - 2\nu, \zeta) \right] \frac{\nu d\nu}{\pi i},
\end{aligned}$$

(58)

But

$$\begin{aligned}
&\frac{\Gamma(a_\nu^+)}{\Gamma(b_\nu^+)} \zeta^{\nu} M(a_\nu^+, 1 + 2\nu, \zeta) - \frac{\Gamma(a_\nu^-)}{\Gamma(b_\nu^-)} \zeta^{-\nu} M(a_\nu^-, 1 - 2\nu, \zeta) \\
&= \frac{\Gamma(a_\nu^+)}{\Gamma(b_\nu^+)} \zeta^{\nu} \left[ M(a_\nu^+, 1 + 2\nu, \zeta) - \frac{\Gamma(b_\nu^+) \Gamma(a_\nu^-)}{\Gamma(a_\nu^+) \Gamma(b_\nu^-)} \zeta^{-2\nu} M(a_\nu^-, 1 - 2\nu, \zeta) \right] \\
&= \frac{\Gamma(a_\nu^+)}{\Gamma(b_\nu^+)} \zeta^{\nu} \left[ M(a_\nu^+, b_\nu^+, \zeta) - \frac{\Gamma(b_\nu^+) \Gamma(a_\nu^-)}{\Gamma(a_\nu^+) \Gamma(b_\nu^-)} \zeta^{1-b_\nu^+} M(a_\nu^+ - b_\nu^+ + 1, 2 - b_\nu^+, \zeta) \right]
\end{aligned}$$

From the representation (36),

$$U(a, b, z) = \frac{\Gamma(1-b)}{\Gamma(a-b+1)} \left[ M(a, b, z) + z^{1-b} \frac{\Gamma(b-1)\Gamma(a-b+1)}{\Gamma(a)\Gamma(1-b)} M(a-b+1, 2-b, z) \right]. \quad (59)$$

But

$$\frac{\Gamma(b_\nu^+)}{\Gamma(b_\nu^-)} = -\frac{\Gamma(2\nu)}{\Gamma(-2\nu)} = -\frac{\Gamma(b_\nu^+ - 1)}{\Gamma(1 - b_\nu^+)}$$

Thus,

$$\begin{aligned}
& \frac{\Gamma(a_\nu^+)}{\Gamma(b_\nu^+)} \zeta^{\nu} \left[ M(a_\nu^+, b_\nu^+, \zeta) - \frac{\Gamma(b_\nu^+) \Gamma(a_\nu^-)}{\Gamma(a_\nu^+) \Gamma(b_\nu^-)} \zeta^{1-b_\nu^+} M(a_\nu^+ - b_\nu^+ + 1, 2 - b_\nu^+, \zeta) \right] \\
&= \frac{\Gamma(a_\nu^+)}{\Gamma(b_\nu^+)} \zeta^{\nu} \left[ M(a_\nu^+, b_\nu^+, \zeta) + \zeta^{1-b_\nu^+} \frac{\Gamma(b_\nu^+ - 1) \Gamma(a_\nu^-)}{\Gamma(a_\nu^+) \Gamma(1 - b_\nu^+)} M(a_\nu^+ - b_\nu^+ + 1, 2 - b_\nu^+, \zeta) \right] \\
&= \zeta^{\nu} \frac{\Gamma(a_\nu^+)}{\Gamma(b_\nu^+)} \left[ M(a_\nu^+, b_\nu^+, \zeta) + \zeta^{1-b_\nu^+} \frac{\Gamma(b_\nu^+ - 1) \Gamma(a_\nu^+ - b_\nu^+ - 1)}{\Gamma(a_\nu^+) \Gamma(1 - b_\nu^+)} M(a_\nu^+ - b_\nu^+ + 1, 2 - b_\nu^+, \zeta) \right] \\
&= \zeta^{\nu} \frac{\Gamma(a_\nu^+) \Gamma(a_\nu^-)}{\Gamma(b_\nu^+) \Gamma(1 - b_\nu^+)} U(a_\nu^+, b_\nu^+, \zeta),
\end{aligned}$$

where the last equality follows from (59). Using this last equality and (56), now (58) reads

$$\begin{aligned}
G(\tau, y, y') &= (y')^{-2} R^{-1} (Ry')^{(1+\omega)/2} e^{-\theta y'} e^{-\gamma(y+y')} \zeta^{(1-\omega)/2} e^{-(1-\omega)^2 \tau/4} \\
&\times \int_0^\infty e^{-\nu^2 \tau} \frac{\Gamma(a_\nu^+) \Gamma(a_\nu^-)}{\Gamma(2i\nu) \Gamma(-2i\nu)} (\zeta \zeta')^{\nu} U(a_\nu^+, b_\nu^+, \zeta) U(a_\nu^+, b_\nu^+, \zeta') \frac{d\nu}{2\pi}, \\
&= (y')^{\omega-2} (yy')^{(1-\omega)/2} e^{-\gamma y} e^{-(\theta+\gamma)y'} e^{-(1-\omega)^2 \tau/4} \\
&\times \int_0^\infty e^{-\nu^2 \tau} \frac{\Gamma(a_\nu^+) \Gamma(a_\nu^-)}{|\Gamma(2i\nu)|^2} (\zeta \zeta')^{\nu} U(a_\nu^+, b_\nu^+, \zeta) U(a_\nu^+, b_\nu^+, \zeta') \frac{d\nu}{2\pi}, \tag{60}
\end{aligned}$$

The relation (60) gives the continuous spectrum contribution to  $G(\tau, y, y')$ . The computation has been done assuming  $y \leq y'$ , but the reader can repeat it for  $y \geq y'$  and find (60) again. Also, remember that we treat two cases: Case 1, where  $1 \leq \omega < \infty$  and Case 2, where  $0 \leq \omega < 1$ . We will establish below that, for Case 2, the continuous spectrum contribution is the sole contribution. Accepting that, we can summarize at this point with

Spectral solution, Case 2 ( $0 \leq \omega < 1$ ):

$$\begin{aligned}
G_c(\tau, y, y') &= (y')^{\omega-2} (yy')^{(1-\omega)/2} e^{-\gamma y} e^{-(\theta+\gamma)y'} e^{-(1-\omega)^2 \tau/4} \int_0^\infty \phi_\nu(y, y') e^{-\nu^2 \tau} d\nu, \\
&\text{using } R = \frac{1}{2} \sqrt{\theta^2 + 4c}, \quad \gamma = -\frac{1}{2}(\theta - \sqrt{\theta^2 + 4c}), \quad \psi = \frac{\omega\gamma}{R}, \\
&\quad a_\nu = \frac{1}{2}(1 - \omega) + \psi + i\nu, \quad b_\nu = 1 + 2i\nu, \\
\text{and } \phi_\nu(y, y') &= \frac{1}{2\pi} \frac{\Gamma(a_\nu) \Gamma(a_\nu - \nu)}{|\Gamma(2i\nu)|^2} (R^2 yy')^{\nu} U(a_\nu, b_\nu, Ry) U(a_\nu, b_\nu, Ry').
\end{aligned}$$

(61)

**Remarks.**

(i) The subscript ‘c’ in (61) refers to the ‘continuous’ spectrum, which is the entire spectrum under Case 2. Later, we use ‘d’ for the ‘discrete’ spectrum contribution.

(ii) Recall that the speed density  $m(y)$  associated to a diffusion is proportional to the stationary density, given for our problem at (12). If you remove  $m(y') \propto (y')^{\omega-2} e^{-\theta y'}$  from (61), what remains is invariant under  $y \leftrightarrow y'$ , a well-known general property of diffusions.

## 9.2 Spectral solution, Case 1

Referring to Fig. 1, let  $\mathcal{C}$  denote the entire (counter-clockwise) closed contour and  $\Omega$  the open interior bounded by  $\mathcal{C}$ . In addition to the identified branch cut singularity at  $s = s_c$ ,  $\hat{G}(s, y, y')$  may have simple pole singularities at various  $s_n \in \Omega$ . In that case, applying the Residue Theorem generalizes (54) to:

$$G(\tau, y, y') = \int_{\Gamma} \frac{ds}{2\pi i} e^{s\tau} \hat{G}(s, y, y') = G_c(\tau, y, y') + \sum_{s_n \in \Omega} e^{s_n \tau} \text{Res}[\hat{G}(s_n, y, y')]. \quad (62)$$

Here

$$\text{Res}[\hat{G}(s_n, y, y')] := \lim_{s \rightarrow s_n} (s - s_n) \hat{G}(s, y, y')$$

denotes the simple pole residue of  $\hat{G}$  at  $s_n$  and  $G_c$  is already given at (61). The next step is locating these putative poles.

Looking at (53), there are potentially poles lurking in  $M(a_s, b_s, \zeta)$  and  $\Gamma(a_s)$ . However, while  $M(a, b, z)$  has a simple pole at  $b = -n$ , where  $n$  is a positive integer (see [1]) the function actually appears in the regularized form  $M(a, b, \zeta)/\Gamma(b)$ , which is everywhere regular. This leads us to seek possible poles in  $\Gamma(a_s)$ , which has simple poles should  $a_s = -n$ , where  $n = 0, 1, 2, \dots$ , here a generally terminating sequence. These poles correspond to the vanishing of the Wronskian in (52). More specifically, we have the

$$\text{pole criteria: } s = s_n, \text{ such that } a(s_n) = -n, \text{ (} n = 0, 1, 2, \dots \text{) and } s \in \Omega. \quad (63)$$

As we shall see, assuming  $1 \leq \omega < \infty$  (Case 1) and dependent upon the other parameters, there may exist zero or a finite number of such  $s_n$ .

### 9.2.1 Sub-case: real parameters

It is helpful to begin with the sub-case where all the parameters  $(\omega, \theta, c)$  are real, with  $\omega \geq 1$ ,  $c \geq 0$  and  $\theta$  of any sign. In that case, from (53),

$$a(s) = r(s) + \psi = \frac{1}{2}(1 - \omega) + \frac{1}{2}\sqrt{(1 - \omega)^2 + 4s} + \psi,$$

where  $\psi = \omega\gamma/R \geq 0$ . Notice that  $\psi$  is real, non-negative, and *independent of  $s$* . To find  $a(s) = -n$ , we must have  $r(s) = \frac{1}{2}(1 - \omega) + \frac{1}{2}\sqrt{(1 - \omega)^2 + 4s}$  both real and non-positive. For  $r(s)$  to be real, we must have  $s$  real and lying on the real

$s$ -axis with  $s \geq s_c$ . Since  $\omega \geq 1$ , at  $s = 0$ , we have  $r(0) = \frac{1}{2}[(1-\omega) + (\omega-1)] = 0$ . For  $s > 0$ , we have  $r(s) > 0$ . Hence,  $r(s)$  is both real and negative only when  $s \in [s_c, 0]$ . For emphasis:

- *under real parameters, the only possible poles (the discrete spectra) lie on the negative real  $s$ -axis in-between the branch cut at  $s = s_c = -(\omega - 1)^2/4$  and the origin.*

The reader should picture a graph of  $a(s)$  as  $s$  increases from  $s_c$  to 0. Suppose  $\psi > 0$ , so that  $a(0) = \psi > 0$ . Suppose  $\omega$  is sufficiently large so that  $a(s_c) = (1 - \omega)/2 + \psi < 0$ . Finally, note that, for  $s \in (s_c, 0)$ ,

$$a'(s) = \frac{1}{\sqrt{(1-\omega)^2 + 4s}} > 0.$$

Thus,  $a(s)$  is monotone increasing over  $s \in [s_c, 0]$  and, under the assumptions, crosses the  $s$ -axis exactly once within the interval. That crossing point is the location of the pole  $s_0$  where  $a(s_0) = 0$ .

Under these same assumptions, is there a pole  $s_1$  – i.e., a value of  $s$  where  $a(s_1) = -1$ ? For this to be true,  $\omega$  would have to be even larger, now sufficiently large so that  $a(s_c) = (1 - \omega)/2 + \psi + 1 < 0$ . If this last relation holds, then by the same argument, there is a unique point  $s_1 \in [s_c, 0]$  such that  $a(s_1) = -1$ . It may be helpful to think of the relation  $a(s_c) = (1 - \omega)/2 + \psi + 1 < 0$  as simply a version of our previous relation (for  $s_0$ ) except we have  $\psi \rightarrow \psi + 1$ . Moreover, by picturing how the graph of  $a(s)$  shifts vertically as  $\psi \rightarrow \psi + 1$ , one sees that, when the putative  $s_1$  exists, then *so does  $s_0$  and  $s_1 < s_0$* .

The case of general  $n$  for  $n$  any positive integer should be clear. To have  $a(s_n) = -n$ ,  $\omega$  must be sufficiently large so that  $a(s_c) = (1 - \omega)/2 + \psi + n < 0$ . When that last relation holds, there is a unique point  $s_n \in [s_c, 0]$  such that  $a(s_n) = -n$ . Moreover, when the putative  $s_n$  exists, then so do all the  $s_m$  for  $m = 0, 1, \dots, n - 1$ . In addition, these real poles are ordered in the permissible interval  $[s_c, 0]$  such that

$$s_c \leq s_n < s_{n-1} < \dots < s_0 \leq 0. \quad (64)$$

What is the condition for at least one pole? As we have seen, for  $s_0$  to exist, we must have  $(1 - \omega)/2 + \psi < 0$ ; i.e.,

$$\text{for a discrete spectrum to exist, one needs } (\omega - 1)/2 > \psi \geq 0. \quad (65)$$

As promised, (65) shows there is no discrete spectrum for Case 2 ( $0 \leq \omega < 1$ ) – at least for the real parameter sub-case.

What is  $n_{max}$ , the largest value of  $n$  in (64)? It is the largest integer such that  $(1 - \omega)/2 + \psi + n < 0$ . Let  $\lfloor x \rfloor$  denote the largest integer contained in  $x$  under the assumption that  $x \geq 0$ . Then we have found that

$$\text{provided (65) holds, } n_{max} = \lfloor (\omega - 1)/2 - \psi \rfloor \geq 0. \quad (66)$$



Finally, provided (65) holds and  $n \leq n_{max}$ , what is  $s_n$ ? The relation  $a(s_n) = -n$  is easily solved for  $s_n$  to yield

$$s_n = (n + \psi)^2 + (1 - \omega)(n + \psi) \quad (n = 0, 1, \dots, n_{max}). \quad (67)$$

Summarizing at this point we have now developed (62) to

$$G(\tau, y, y') = G_c(\tau, y, y') + 1_{\{\frac{\omega-1}{2} > \psi\}} \sum_{n=0}^{n_{max}} e^{s_n \tau} \text{Res}[\hat{G}(s_n, y, y'), \quad (68)$$

where  $s_n$  is found in (67) and  $n_{max}$  is found in (66). It remains to calculate the required residues at these poles.

### 9.2.2 Residues

From (53), since  $a(s) = r(s) + \psi$ , we have  $r_n := r(s_n) = -(n + \psi)$ . Since  $b(s) = \omega + 2r(s)$ , we have  $b_n := b(s_n) = \omega + 2r_n$ . Recalling that  $M(a, b, z)/\Gamma(b)$  is regular everywhere, we have

$$\lim_{s \rightarrow s_n} \frac{1}{\Gamma(b_s)} M(a_s, b_s, \zeta) = \frac{1}{\Gamma(b_n)} M(-n, b_n, \zeta),$$

where  $\zeta$  denotes either  $Ry$  or  $Ry'$ . Also, from the  $U$  representation (36),

$$\lim_{s \rightarrow s_n} U(a_s, b_s, \zeta') = \frac{\Gamma(1 - b_n)}{\Gamma(1 - n - b_n)} M(-n, b_n, \zeta'),$$

since the pole in  $\Gamma(a(s_n))$  suppresses the second factor of  $M$ . Here  $\zeta'$  denotes  $Ry'$  when  $\zeta = Ry$  and vice-versa.

Recall that, as  $z \rightarrow -n$ ,

$$\Gamma(z) \approx \frac{(-1)^n}{n!} \frac{1}{z + n}, \quad (n = 0, 1, 2, \dots).$$

Thus, as  $s \rightarrow s_n$

$$\Gamma(a(s)) \approx \frac{(-1)^n}{n!} \frac{1}{a'(s_n)(s - s_n)} = \frac{(-1)^n}{n!} \frac{(\omega - 1 - 2n - 2\psi)}{(s - s_n)}.$$

Putting it all together we have, as  $s \rightarrow s_n$ ,

$$\begin{aligned} \hat{G}(s, y, y') &\approx \frac{(-1)^n}{n!} \frac{(\omega - 1 - 2n - 2\psi)}{(s - s_n)} \frac{(b_n)_n}{\Gamma(b_n)} R^{\omega-1+2r_n} y^{r_n} (y')^{r_n+\omega-2} e^{-\gamma y} e^{-(\gamma+\theta)y'} \\ &\times M(-n, b_n, Ry) M(-n, b_n, Ry'), \end{aligned}$$

where we have written  $\Gamma(1 - b_n)/\Gamma(1 - n - b_n) = (-1)^n (b_n)_n$  using the Pochhammer symbol. Factoring out the stationary density, we have found that

$$\begin{aligned} \text{Res}[\hat{G}(s, y, y')] &= R (Ry')^{\omega-2} e^{-\theta y'} \frac{(\omega - 1 - 2n - 2\psi) (b_n)_n}{n! \Gamma(b_n)} \\ &\quad \times (R^2 y y')^{r_n} e^{-\gamma(y+y')} M(-n, b_n, Ry) M(-n, b_n, Ry'). \end{aligned}$$

Summarizing, with real parameters, we have fleshed out (62) to read

$$\boxed{\begin{aligned} G(\tau, y, y') &= G_c(\tau, y, y') \\ &+ R (Ry')^{\omega-2} e^{-\theta y'} e^{-\gamma(y+y')} \times 1_{\{\frac{\omega-1}{2} > \psi\}} \sum_{n=0}^{\lfloor (\omega-1)/2-\psi \rfloor} \phi_n(y, y') e^{s_n t} \end{aligned}} \quad (69)$$

where

$$\phi_n(y, y') = \frac{(\omega - 1 - 2n - 2\psi) (b_n)_n}{n! \Gamma(b_n)} (R^2 y y')^{r_n} M(-n, b_n, Ry) M(-n, b_n, Ry'),$$

and using the other notations above. The expression (69) completes the proof of Theorem 1 for the case of real parameters.

### 9.2.3 General case: complex parameters

As we saw in Sec. 2.1, complex parameters arise under the reduction of the bivariate XGBM model to (9). For example, recall what happens when trying to calculate option values under the risk-neutral (Q) model. Then, one has the mapping of equation (21). That is,  $(\theta, c) \rightarrow (\theta_z^+, c_z^-)$  where  $z$  is in the preferred Fourier inversion strip ( $0 < \Im z < 1$ ) and

$$\theta_z^+ = \frac{2}{\xi^2} (\theta + 1z\rho\xi), \quad c_z^- = \frac{1}{\xi^2} (z^2 - 1z). \quad (70)$$

With these changes,  $\hat{G}$  in (53) still ‘works’. Since  $\omega$  remains real under these complexifications, the spectral solution components  $G_c(\tau, y, y')$  remains the same: the location of both the branch point at  $s = s_c = -(1 - \omega)^2/4$  and the associated branch cut is unchanged.<sup>9</sup> What does change is that the formerly non-negative parameter  $\psi$  should now be considered complex; it remains  $s$ -independent. Now at fixed  $z$ :

$$\psi \rightarrow \psi_z = \frac{\omega\gamma_z}{R_z} = \frac{\omega}{2} \left( 1 - \frac{\theta_z^+}{\sqrt{(\theta_z^+)^2 + 4c_z^-}} \right)$$

With complex  $\psi_z$ , let’s write again the pole criteria (63), which reads

pole criteria:  $s = s_n$ , such that

$$\sqrt{(\omega - 1)^2/4 + s} = \frac{1}{2}(\omega - 1) - n - \psi_z, \quad (n = 0, 1, 2, \dots) \text{ and } s \in \Omega. \quad (71)$$

<sup>9</sup>More carefully, by ‘the same’, I mean the *formula* for  $G_c(\tau, y, y')$  continues to be (61), already derived allowing complex values for  $(R, \gamma, \psi)$ .

For any complex number  $\zeta$ , then  $\sqrt{\zeta}$  has a branch point singularity at the origin. With the branch cut conventionally placed along the negative  $\zeta$ -axis, then in the cut plane  $\zeta = R e^{i\phi}$  with  $-\pi < \phi < \pi$ . Thus  $\sqrt{\zeta} = \sqrt{R} e^{i\phi/2}$ , which shows  $\Re \sqrt{\zeta} > 0$  for all  $R > 0$ . This applies to our situation (71) with the identification  $\zeta = s - s_c = s + (\omega - 1)^2/4$ . In other words, since  $\Re \sqrt{\zeta} > 0$  in the cut  $s$ -plane, we can take the real part of both sides of (71) to find that

$$\frac{1}{2}(\omega - 1) - n - \Re \psi_z > 0 \Rightarrow n < \frac{1}{2}(\omega - 1) - \Re \psi_z \quad (72)$$

For a non-empty discrete spectrum, we need a solution  $s \in \Omega$  to (71) for  $n = 0$ . That requires  $\frac{1}{2}(\omega - 1) > \Re \psi_z$  to be satisfied. The poles themselves are still given by the same formula (67), now

$$\boxed{\begin{aligned} s_n = s_n(z) &= (n + \psi_z)^2 + (1 - \omega)(n + \psi_z), \quad (n = 0, 1, \dots, n_{max}), \\ \text{where } n_{max} &= \lfloor \frac{1}{2}(\omega - 1) - \Re \psi_z \rfloor. \end{aligned}} \quad (73)$$

The same formulas as before still hold for the residues. Thus, we have the generalization, with complex parameters:

$$\boxed{\begin{aligned} G(\tau, y, y') &= G_c(\tau, y, y') \\ &+ R(Ry')^{\omega-2} e^{-\theta y'} e^{-\gamma(y+y')} \times 1_{\{\frac{\omega-1}{2} > \Re \psi\}} \sum_{n=0}^{\lfloor (\omega-1)/2 - \Re \psi \rfloor} \phi_n(y, y') e^{s_n \tau} \end{aligned}} \quad (74)$$

where

$$\phi_n(y, y') = \frac{(\omega - 1 - 2n - 2\psi)(b_n)_n}{n! \Gamma(b_n)} (R^2 y y')^{r_n} M(-n, b_n, Ry) M(-n, b_n, Ry').$$

Comparing (74) to the previous (69), the formulas are very close – the only change is  $\psi \rightarrow \Re \psi$  in the pole condition and sum limit.

**Complications induced by the Fourier inversion.** When using the above formulas for the bivariate model, as we have discussed, the parameter  $\psi_z$  depends upon the Fourier parameter  $z$ . For each fixed  $z$ , when  $\omega - 1 > 2 \Re \psi_z$ , the number of discrete eigenvalues  $N_e(z)$  is given from the above by  $N_e(z) = 1 + \lfloor (\omega - 1)/2 - \Re \psi_z \rfloor$ . Thus, when integrating along a contour in the complex  $z$ -plane to implement (26), you will often find  $N_e(z)$  changing by unit steps along the integration contour.

An example should make this clear. Take the risk-neutral XGBM option model with  $\omega = 3$ ,  $\theta = 4$ ,  $\rho = -0.8$ , and  $\xi = 1$ . To find option values, we perform a Fourier inversion by integrating along  $z = x + i/2$  for  $x \in [0, \infty)$ . Fig. 5 plots the number of eigenvalues (number of elements in the discrete spectrum) as  $x$  varies along this contour. As you can see, at the beginning of the contour ( $x = 0$ ), there are 3 eigenvalues in the spectrum, but they each subsequently drop out as  $x$  increases, at *transition points*  $x \approx (5.80, 33.42, 120.02)$ . Thus, at large  $x$ , indeed for all  $x > 120.02$ , the discrete spectrum is empty.

What is going on that causes the drop-outs? If you look at trajectory plots of  $s_n(z)$  in the complex  $s$ -plane (as  $z$  varies), you will find that the drop-outs occur precisely where the  $s_n(z)$  *touch the branch cut* (Fig. 2).

Note that the branch-cut itself is *not* in the region  $\Omega$ . Thus, the qualification  $s \in \Omega$  in (71) is important and is enforced by the behavior we have just described. Eigenvalues reaching the branch cut is a new feature of the complex parameter case. With real parameters,  $s_n(z)$  can approach the cut – but only from the real axis. So, if it reached the cut, it would reach it at the branch point end-point only, where the formulas tend to be smoother.

A complication associated with this behavior is that the two components of the spectral expansions above (discrete and continuous) can show discontinuities at these transition points – even though their sum is smooth. While  $G(\tau, y, y'; z)$  itself will be smooth as  $z$  passes through a transition value, there may be offsetting discontinuities in the (continuous and discrete) components  $G_c$  and  $G_d$  or associated functions. Examples of associated functions to  $(G, G_c, G_d)$  are the marginals  $(H, H_c, H_d)$  in which the terminal volatility  $y'$  is integrated out. See Fig. 3 for examples of how the branch cut touches of Fig. 2 manifest themselves in discontinuities of  $H_c$  and  $H_d$ , while  $H$  remains continuous in  $z$ . This behavior needs to be carefully handled in any coding implementation: we discussed our particular method in Sec. 7.

## 10 Appendix B – The SABR model limit

If one drops the drifts from (1), the system becomes

$$\begin{cases} dS_t = \sigma_t S_t dB_t, & S_t \in \mathbb{R}_+, \\ d\sigma_t = \xi \sigma_t dW_t, & \sigma_t \in \mathbb{R}_+, \\ dB_t dW_t = \rho dt, \end{cases} \quad (75)$$

which is the lognormal SABR model. Equivalently, (2) becomes

$$\begin{cases} dX_t = -\frac{1}{2}Y_t^2 dt + Y_t dB_t, & X_t \in \mathbb{R}, \\ dY_t = \xi Y_t dW_t, & Y_t \in \mathbb{R}_+, \\ dB_t dW_t = \rho dt. \end{cases} \quad (76)$$

Now, (11) holds with  $\omega = 0$ ,  $\theta_z^- = -2\nu\rho/\xi$ , and  $c_z^+ = (z^2 + \nu z)/\xi^2$ . Tracing the implications in Theorem 1, there are considerable simplifications. Using the notations there, since  $\omega = \psi = 0$ , there is no discrete spectrum contribution. In the continuous spectra integrand, the key simplification is the relation (see [1]):

$$U\left(\frac{1}{2} + \nu, 1 + 2\nu, z\right) = \frac{e^z z^{-\nu}}{\sqrt{\pi}} K_{\nu}\left(\frac{z}{2}\right),$$

where  $K_{\nu}(z)$  is a modified Bessel function. One can also show from [1] that

$$\left| \frac{\Gamma(\frac{1}{2} + \nu)}{\Gamma(2\nu)} \right|^2 = 4\nu \sinh \pi\nu.$$

Putting it all together, (11) reduces to

$$\begin{aligned} p_{SABR}(t, x', y' | x, y) &= \frac{1}{\pi^3} \frac{y^{1/2}}{(y')^{3/2}} e^{-\frac{1}{8}\xi^2 t} \times \\ &\int_{-\infty}^{\infty} \int_0^{\infty} e^{-\frac{1}{2}\nu^2 \xi^2 t} \nu (\sinh \pi\nu) K_{\nu}(\chi_z y) K_{\nu}(\chi_z y') e^{-\nu z[(x-x') - (\rho/\xi)(y-y')]} d\nu dz, \\ &\text{using } \chi_z = [(1 - \rho^2)z^2 - \nu z]^{1/2}. \end{aligned} \quad (77)$$

Eqn (77) agrees with a representation for the SABR transition density previously found in [6] (Ch. 8, eqn (8.81)). Note that in (77) I have flipped the sign of dummy integration variable  $z$  relative to (11) to make the comparison with [6].

## 11 Appendix C – The martingale defect

The XGBM model under the risk-neutral (Q-measure) evolution is given at (16). Using  $(\omega_Q, \theta, \xi, \rho)$  from there, define  $\beta = 2 - 2\omega_Q/\xi^2$ , and  $\gamma = 2[(\rho/\xi) - (\theta/\xi^2)]$ . We also need  $a_\mu = (\beta - 1)/2 + \mu$ ,  $c_\mu = 1 + 2\mu$ ,  $c_m = \beta - 2 - 2m$ , and  $d_m = c_m - 1$ . Then, one can show that the martingale defect under that model is given by

$$\mathbb{E}_{S_0, \sigma_0} \left[ \frac{S_t}{S_0} \right] = \begin{cases} 1 & \gamma \leq 0 \quad (\text{i.e., } -1 \leq \rho \leq \theta/\xi), \\ 1 - A(\sigma_0, t), & \gamma > 0 \quad (\text{i.e., } \theta/\xi < \rho \leq 1). \end{cases} \quad (78)$$

Here  $A(x, t)$  is an absorption probability, given by:

$$A(x, t) = A_\infty(x) + A_d(x, t) + A_c(x, t), \quad (79)$$

$$\text{where } A_\infty(x) = \begin{cases} 1 - \frac{\Gamma(\beta-1, \gamma x)}{\Gamma(\beta-1)}, & \beta > 1, \\ 1, & \beta < 1, \end{cases} \quad (80)$$

$$\begin{aligned} A_d(x, t) &= 1_{\{\beta > 3\}} e^{-\gamma x} \sum_{m=0}^{[(\beta-3)/2]} \frac{(-1)^{m+1} (\gamma x)^{\beta-2-m}}{m! \Gamma(d_m)} \\ &\times \frac{\exp\{-\frac{1}{2}[\beta - 2 + m(\beta - 3 - m)]\xi^2 t\}}{[\beta - 2 + m(\beta - 3 - m)]} M(-m, c_m, \gamma x), \end{aligned} \quad (81)$$

$$\text{and } A_c(x, t) = - \int_0^\infty \bar{g}(\mu) \eta(\gamma x, \mu) \exp\left\{-\frac{1}{2}\left[\mu^2 + \frac{(\beta-1)^2}{4}\right]\xi^2 t\right\} d\mu, \quad (82)$$

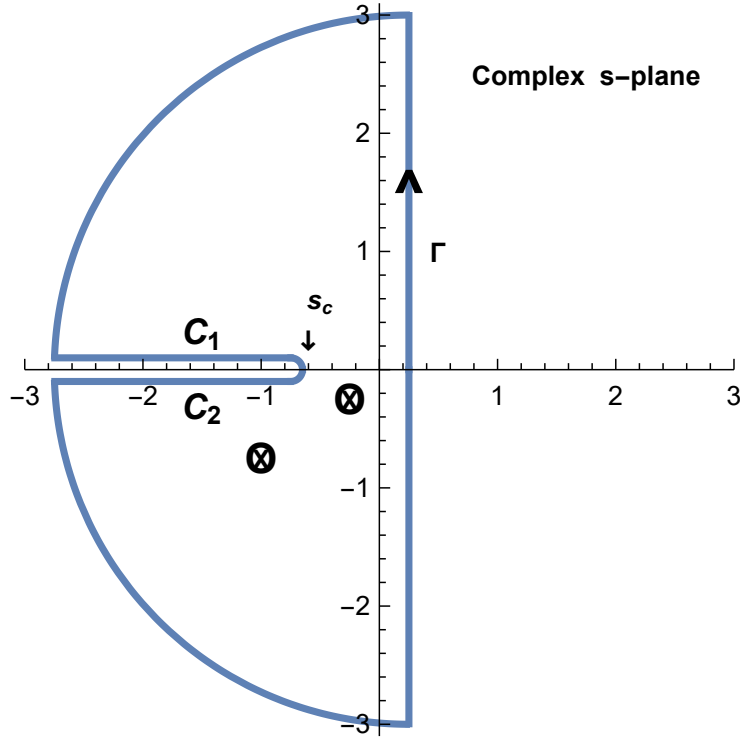
$$\text{using } \bar{g}(\mu) = \frac{1}{2\pi} \left| \frac{\Gamma(c_\mu - a_\mu)}{\Gamma(2\mu)} \right|^2 \frac{1}{\mu^2 + \frac{(\beta-1)^2}{4}},$$

$$\text{and } \eta(y, \mu) = e^{-y} y^{a_\mu} U(c_\mu - a_\mu, c_\mu, y).$$

Proof: Follows easily from the absorption probability found in Sec 13.2.9 of Ch. 13 of [6].

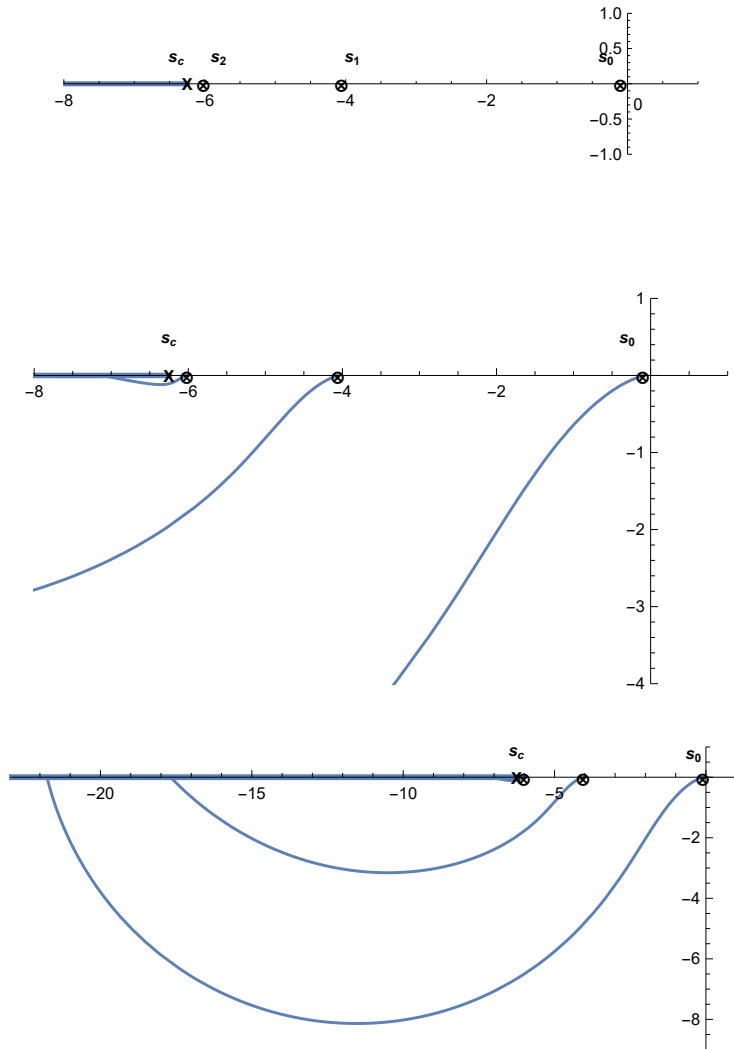
**Remarks.** As discussed in [5], an alternative route to the martingale defect is the relation  $\mathbb{E}_{S_0, \sigma_0} \left[ \frac{S_T}{S_0} \right] = H(T, \sigma_0; z = i)$ . Showing the equivalence of this last relation to (78) is a good exercise for the interested reader when  $T \rightarrow \infty$ . A direct check for general  $T$  has eluded us.

Figure 1: Green function inversion contour in the complex  $s$ -plane



**Notes.** The vertical contour  $\Gamma$  is the Bromwich (Laplace) inversion contour in the complex  $s$ -plane for the auxiliary Green function  $G$ . The Residue Theorem converts the integral along  $\Gamma$  into an integral along the branch-cut (which extends along the line  $s \in (-\infty, s_c)$  plus contributions from poles (shown as crossed-circles). The figure is schematic: there generally may be zero or more poles. The branch-cut endpoint is at  $s_c = -\frac{1}{4}(1 - \tilde{\omega})^2 \leq 0$ , where  $\tilde{\omega} = 2\omega/\xi^2$ . The poles move in the  $s$ -plane as the separate Fourier inversion parameter  $z$  moves in the complex  $z$ -plane. However, as  $z$  changes (while other parameters are fixed), the branch-cut endpoint  $s_c$  remains fixed.

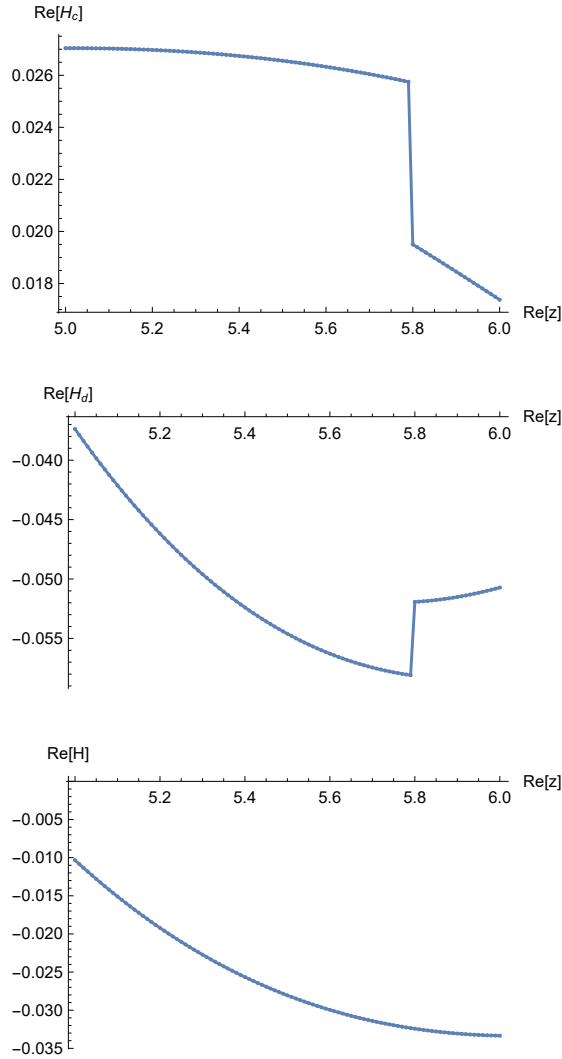
Figure 2: Eigenvalue Trajectories  $s_n(z)$  in the Complex  $s$ -plane vs.  $z$



**Notes.** Parameters:  $\omega = 3$ ,  $\theta = 4$ ,  $\rho = -0.8$ , and  $\xi = 1$ . Fourier integration is along the contour  $z = 1/2 + x$ , where at most 3 eigenvalues  $s_n(x)$ , ( $n = 0, 1, 2$ ) contribute. Top chart shows the  $s_n(0)$ . Bottom chart shows parametric plots of  $s_n(x)$  as  $x$  increases along the contour. Middle chart shows detail to make the  $s_2(x)$  trajectory clearer. The trajectories touch the branch cut and the corresponding eigenvalues disappear from the solution at  $x_n \approx \{5.796, 33.424, 120.017\}$  for  $\{s_2, s_1, s_0\}$  respectively.



Figure 3: **Continuous, Discrete, and Full Fundamental Transform:**  
 $\Re H(z = i/2 + x)$  vs.  $x$



**Notes.** Model parameters as in Fig.2. The trajectory for the eigenvalue  $s_2(z)$  along the Fourier integration contour  $z = i/2 + x$  touches the branch cut at  $\Re z = x_2 \approx 5.796$ . At that point the fundamental transform  $H(z) = H_c(z) + H_d(z)$  is regular (smooth), while the continuous and discrete components,  $H_c(z)$  and  $H_d(z)$  respectively, have offsetting jumps. This behavior occurs whenever a discrete eigenvalue  $s_n(z)$  touches the  $s$ -plane branch cut as it leaves the solution.

Figure 4: Large T behavior of the Implied Volatility

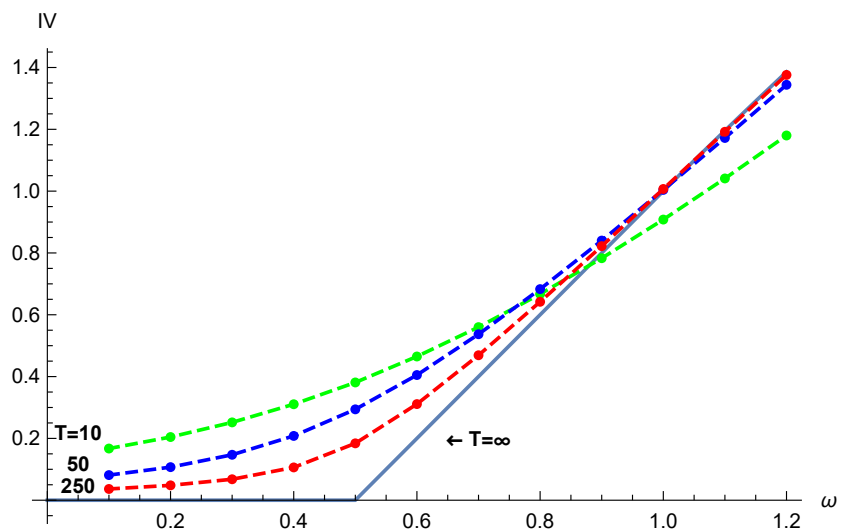


Figure 5: Discrete Spectrum Size along a Fourier Integration Contour

